Spring 2018

Circularly Polarized Two-Dimensional Microstrip Standing-Wave Array Antenna

Yang Fan
Southern Methodist University, yangf@smu.edu

CIRCULARLY POLARIZED TWO-DIMENSIONAL MICROSTRIP

STANDING-WAVE ARRAY ANTENNA

Approved by:

_____

Prof. Choon S. Lee
Associate Professor of Electrical Engineering

_____

Prof. Jerome Butler
Distinguished Professor of Electrical Engineering

_____

Prof. Ping Gui
Professor of Electrical Engineering

_____

Prof. Duncan MacFarlane
Professor of Electrical Engineering

_____

Prof. David Willis
Associate Professor of Mechanical Engineering

CIRCULARLY POLARIZED TWO-DIMENSIONAL MICROSTRIP STANDING-WAVE ARRAY ANTENNA

A Dissertation Presented to the Graduate Faculty of

Bobby B. Lyle School of Engineering

Southern Methodist University

in

Partial Fulfillment of the Requirements

for the degree of

Doctor of Philosophy

with a

Major in Electrical Engineering

by

Yang Fan

M.S., Electrical Engineering, Southern Methodist University

B.S, Electrical Engineering, University of Electrical Science and Technology of China

May 19, 2018

ACKNOWLEDGMENTS

First and foremost, I want to thank my advisor, Dr. Lee. It has been an honor to be your Ph.D. student. You have taught me with patience, motivation, and immense knowledge. I appreciate your contributions of time, ideas, and funding, which have made my Ph.D. experience productive, and your guidance has allowed me to grow as a research scientist.

In addition to my advisor, I would also like to thank the rest of my committee members: Dr. Jerome Butler, Dr. Duncan Macfarlane, Dr. Ping Gui and Dr. David Willis. Your brilliant comments, insightful suggestions, and constant encouragement have been invaluable. In your own ways, you have each added to this project, as well as shaping me as a researcher and a potential world changer.

My sincere thanks also go to Mr. Won Suk and Mr. Gary, who provided me an opportunity to join Samsung Research America as an intern. Your deep insight and valuable experience in the industry encouraged me not only to think broadly about my current research but also to consider future opportunities in this area.

I thank my fellow students, Dr. Ezzat, Mr. Yang Guang, Mr. Linsheng Zhang and Mr. Ayman, for the sleepless nights we worked together at the SMU antenna lab and for all your support over the last four years.

Finally, I owe special thanks to my family for all their love and encouragement—to my parents, who raised me with a love of science and supported me in all my pursuits, and most of the all, to my loving, supportive, encouraging, and beautiful wife, Jiachen, whose faithful support during the final stages of this Ph.D. program I have greatly appreciated. Thank you.

I will count my time at SMU among my life's most valuable memories. I owe thanks to all the people I have met here.

Yang Fan

Southern Methodist University

March 2018

Yang Fan M.S., Electrical Engineering, Southern Methodist University, 2015

Circularly Polarized Two-Dimensional Microstrip
Standing-Wave Array Antenna

Advisor: Associate Professor Choon S. Lee
Doctor of Philosophy conferred, May 19th, 2018
Dissertation completed, April 13th, 2018

The objective of this dissertation is to introduce a novel single-fed circularly polarized (CP) microstrip antenna and extend such a single-feed (SF) scheme to an array structure based on the standing-wave array concept for high-gain applications.

Many practical applications require CP antennas due to their unique characteristics. Compared to linearly polarized radio frequency (RF) waves, CP waves are more resistant to signal degradation due to inclement weather conditions (e.g., rain and snow). In general, obstructions and reflections cannot be avoided in RF communication. Since CP waves are transmitted along all planes, in contrast to the single plane of linearly polarized waves, circular polarization performs better when propagating through obstructions and suffers lower signal strength loss upon reflection. Another important characteristic of CP waves is that a reflected CP wave will travel in the opposite orientation of the incident CP wave, meaning that a right-hand circularly polarized (RHCP) wave will become a left-hand circularly polarized wave (LHCP) after reflection. This specific feature is noteworthy for its use in solving multipath and phasing interference issues. CP antennas are widely used in new 802.11ac 5.8 GHz Wi-Fi systems and unmanned aerial vehicle (UAV) systems;

indeed, an increasing number of companies and institutes are exploring the use of CP antennas with millimeter waves.

Conventionally designed CP antennas require two feeding ports with equal magnitudes but phases 90° apart. Such a two-feed mechanism results in a bulky and expensive structure. Recently, a number of SF options for CP antennas have been proposed. In the Southern Methodist University (SMU) antenna lab, we have created a unique structure for SF CP antennas that shows excellent antenna performance compared to other published results. Due to the square outline and diagonal feeding strategy in this proposed CP patch antenna design, it is feasible to implement the patch in a standing-wave array for high-gain applications requiring a simple, low-profile structure. The standing-wave array antenna developed at SMU has a relatively simple planar structure, is easy to fabricate, and involves low-cost processing.

This dissertation reviews current designs of SF CP microstrip patch antennas and proposes a novel design with improved performance. The structure is similar to a regular microstrip antenna and the design procedure is relatively simple. The basic operational mechanism for CP radiation is based on small apertures in the top radiating patch. Proper arrangement of the aperture holes allows production of two orthogonal degenerate modes, with phases 90° apart from each other but equal magnitudes, resulting in excellent CP radiation. By extending this SF scheme to an array structure based on the standing-wave array concept, a novel circular polarized array antenna can be realized by using one CP patch with standing-wave feeding networks. The standing-wave array antenna developed at SMU has a low-profile planar configuration and a simple feeding network structure and thus can be fabricated easily and cheaply with relatively high gain.

TABLE OF CONTENTS

LIST OF FIGURES

Figure Page

LIST OF TABLES

This is dedicated to Jiachen, my love and a genius in her own right.

CHAPTER 1

INTRODUCTION TO WAVE POLARIZATION AND MICROSTRIP PATCH ANTENNAS

Recent studies in the field of antenna design have shown that there is a high demand for circular polarized antennas with a small size, simple structure, and low fabrication cost that can nonetheless maintain good efficiency and performance and have the potential for integration into arrays for beam-forming. A CP microstrip antenna with a single feed can satisfy the above requirements. Before describing this antenna's design, some basic concepts and definitions that are critical for understanding this dissertation are introduced in Chapter 1.

1.1 Plane Wave

The plane wave model is important and widely used in the electromagnetic engineering field. For example, the RF waves received by an antenna at a sufficiently large distance are usually considered to approximate plane waves. By definition, a plane wave is a wave for which both the electric field and the magnetic field lie in its propagation wave-front (the transverse plane), with the normal in the direction of propagation.

Furthermore, both fields in a transverse plane are perpendicular and have a constant magnitude and phase, as shown in Figure 1.1. For this reason, plane waves are usually called transverse electromagnetic (TEM) waves [1-2].

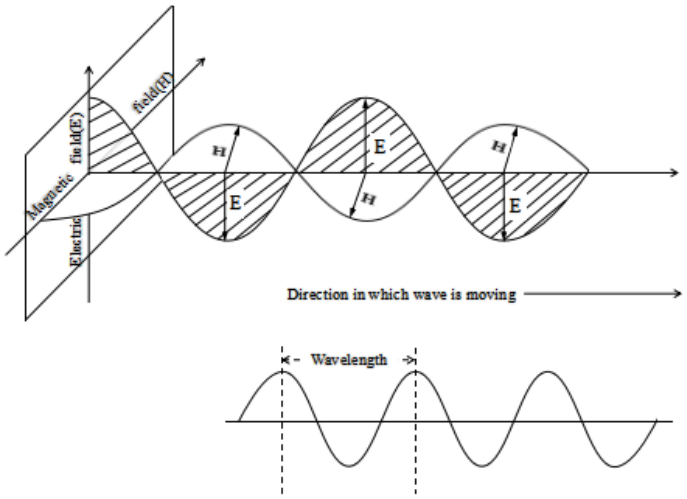

Figure 1.1 Diagram of a plane wave.

1.2 Wave Polarization

1.2.1 Linear Polarization

Wave polarization is the main identifying feature of a plane wave and describes its propagation characteristics. A plane wave is said to be linearly polarized when the direction of the electric field does not change during propagation. For example, consider a plane wave with the following E-field:

$$\boldsymbol{E} = E_0 \cdot e^{-jkz} \cdot e^{j\omega t} \cdot \hat{\boldsymbol{y}} \tag{1.1}$$

The above equation indicates that the wave is propagating in the +z-direction. Moreover, its E-field is oriented in the +y-direction, so the E-field vector is oscillating in the y-direction at angular frequency ω, as shown in Figure 1.2.

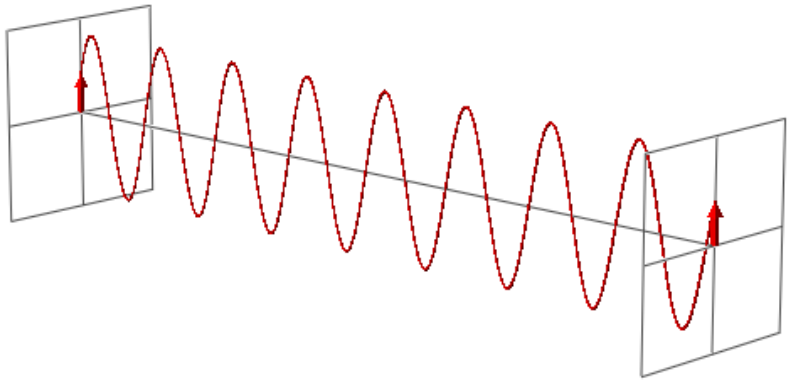

Figure 1.2 Normalized 3D view of the E-field of the plane wave from equation (1.1).

Considering the E-field observed on the wave-front of this plane wave as a function of time, the magnitude of the E-field always oscillates back and forth along the y-axis. Because the oscillation path stays in a single line, this field is linearly polarized [1], as shown in Figure 1.3.

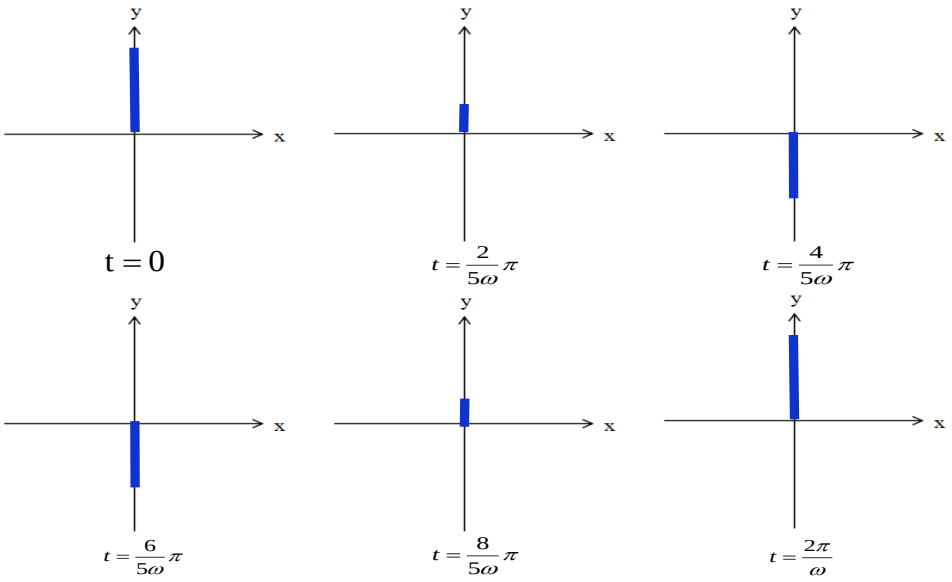

Figure 1.3 Diagram of an E-field along a wave-front at different times.

Linear polarization does not have to occur along the x- or y-axis. For example, consider the plane wave with the following E-field:

$$\boldsymbol{E} = \frac{\sqrt{2}}{2} E_0 \cdot e^{-jkz} \cdot e^{j\omega t} \cdot (\hat{\boldsymbol{x}} + \hat{\boldsymbol{y}}) \tag{1.2}$$

Because the two components of the E-field are in phase—i.e., they have the same frequency and the same initial phase—their combination in the form of the total E-field would also be linearly polarized, as shown in Figure 1.5(a).

1.2.2 Circular Polarization

If the y component of the E-field given in equation (1.2) had a 90° phase difference with the x component, the resulting E-field would be as follows:

$$\boldsymbol{E} = \frac{\sqrt{2}}{2} E_0 \cdot e^{-jkz} \cdot e^{j\omega t} \cdot (\hat{\boldsymbol{x}} + \boldsymbol{e}^{-j\frac{\pi}{2}} \cdot \hat{\boldsymbol{y}}) \tag{1.3}$$

A plane wave with the E-field shown in equation (1.3) would have a CP identity, or circular polarization (Figure 1.4). In a CP E-field, the magnitude of the electric field remains the same but the direction changes such that the tip of the electric field forms a circular shape along its wave-front [3]. Depending on the circulation direction, CP radiation can be either RHCP or LHCP. In practice, the polarization shape is not circular but elliptical. The CP quality is characterized by the axial ratio (AR), which is the ratio of the major to minor E-field magnitude. Thus, the AR of a CP wave should be equal to 1 (linear) or 0 (dB) [2].

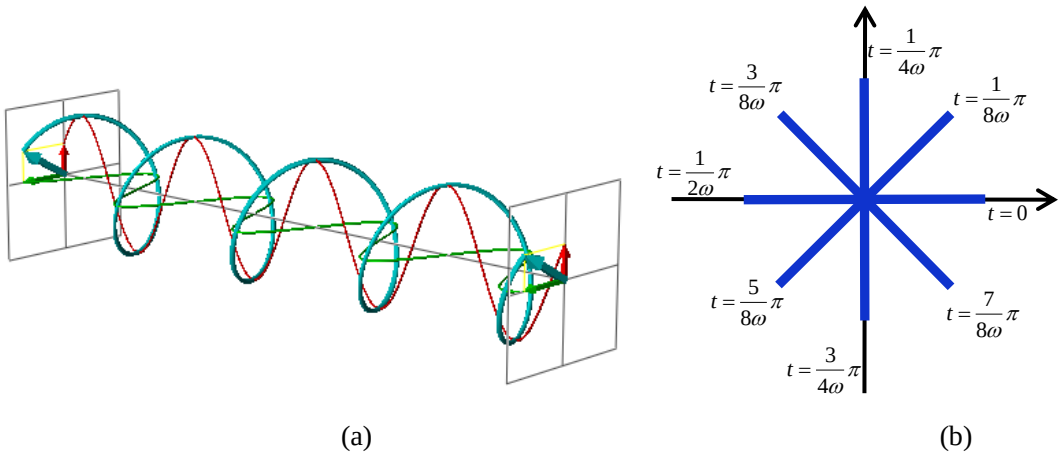

Figure 1.4 (a) Normalized 3D view of the E-field of the plane wave from equation (1.3). (b) Diagram of the E-field on a wave-front at different times.

From equation (1.3), three criteria could be concluded to form circular polarization.

i. The E-field must have two orthogonal components;

ii. The two components must have equal magnitude;

iii. The two components must be 90 degrees out of phase.

Put right thumb pointing to wave travelling direction, if the other four fingers follow the rotating direction of E field, the wave is said to be right hand circularly polarized (RHCP); otherwise, the wave would be left hand circularly polarized (LHCP).

1.2.3 Elliptical Polarization

If a wave can satisfy NO. i and NO. iii requirements in the above three criteria for circular polarization but the magnitude of two components are not equal, it will end up an elliptical shape on the travelling wave front [3], as shown in Figure 1.5(c).

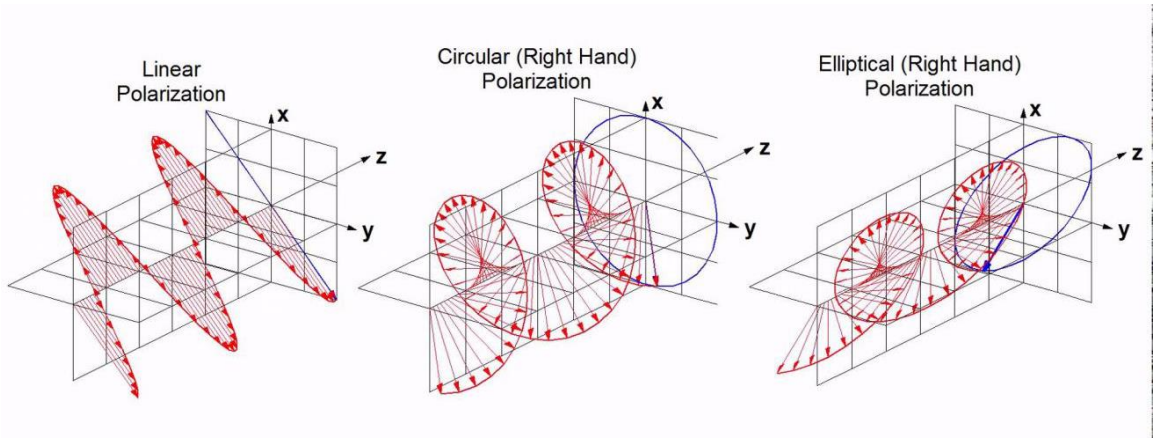

Figure 1.5 3D view of the E-field of the plane wave in: (a) linear; (b) RHCP; (c) RHEP

Finally, in practice, circularly polarized wave is difficult to produce, thus usually it would be slightly elliptical polarized, and in the same way, linearly polarized wave would be elliptical polarized with huge AR value.

1.3 Polarization of Antennas

The antenna polarization is determined by the polarization of the radiated fields it transmits, evaluated in the far field. Thus, antennas are classified as linearly polarized or CP. If an antenna has two polarizations, it is often referred to as "dual-polarized."

The concept of polarization is important for wireless communication due to polarization mismatch. Based on reciprocity, an antenna adopts the same polarization when transmitting and receiving. Thus, for example, an antenna with horizontal polarization (linear polarization parallel to the ground) would not communicate with an antenna with vertical polarization (linear polarization perpendicular to the ground). Therefore, in an RF communication system, the receiving antenna should have the same polarization as the transmitting antenna for the best reception.

The polarization loss factor (PLF) is used to evaluate the power loss due to polarization mismatch [4]. For two linearly polarized antennas, the angle φ represents the acute angle between their polarization directions, and the PLF is defined as follows:

$$PLF = cos^2(\varphi) \tag{1.4}$$

If φ is equal to zero, both antennas will have the same polarization, and there will be no power loss due to polarization mismatch. If φ is equal to 90 degrees, the polarizations of the transmitting and receiving antennas will be perpendicular; no communication will exist between these two antennas, because they cannot receive power from each other.

Hence, one advantage of a CP antenna is that if both antennas have the same circular polarization, the signals transmitted between them will not suffer power loss caused by

polarization mismatch. In addition, according to the reciprocity theorem, an RHCP antenna cannot receive a signal from an LHCP antenna. This represents another advantage of circular polarization, because an RHCP wave will turn into an LHCP wave after experiencing reflection, and the reflected wave would not interfere with the desired incoming wave. Thus, CP antennas have some immunity to the multipath effect.

1.4 Introduction to Microstrip Patch Antennas

The concept of the microstrip antenna was originally developed by Deschamps in the 1950s. However, it was not until the 1970s that the first microstrip antenna was fabricated, thanks to new techniques in substrate manufacturing. Since then, the microstrip antenna has been used in a vast array of applications. Because of their light profiles, low cost, small size and compatibility with highly integrated devices, microstrip antennas have become one of the most commonly used antennas in modern wireless communication systems [5].

1.4.1 Structure of Microstrip Patch Antennas

In general, a microstrip antenna consists of a ground plane, a substrate layer, and a radiating patch, which are combined to form a sandwich structure, as shown in Figure 1.6. A feeding structure transmits energy into the patch to produce radiation.

In Figure 1.6, L and W represent the length and width of the radiating patch, and h is the thickness of the dielectric substrate with relative permittivity ε_r, also known as dielectric constant. In practice, a higher dielectric constant is associated with a smaller antenna patch, but either the efficiency or the bandwidth decreases as a trade-off. The

patch and ground plane are made of a highly conductive metal (typically copper) with thickness t.

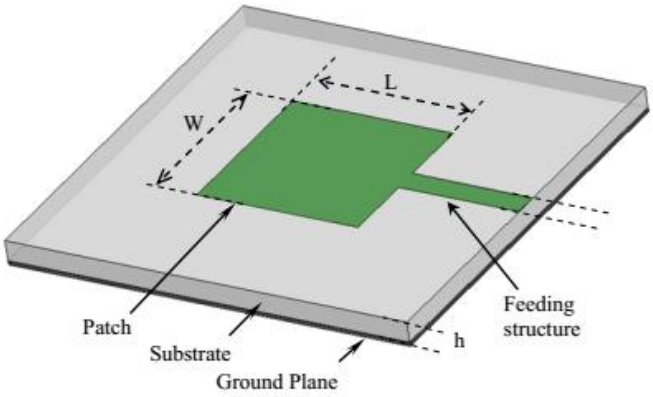

Figure 1.6 A typical microstrip patch antenna.

Generally, the thickness of the metal is not as important as the thickness of the substrate. The substrate thickness is typically much smaller than the free-space wavelength of the desired operational frequency ($h << \lambda_0$), but to maintain the antenna's efficiency, it will not be less than 1/40th of a wavelength. In addition, increasing the substrate thickness with air is a common technique for ultra-wide-band microstrip antenna design [6-9].

1.4.2 Feeding of Microstrip Patch Antennas

The feed method is the most important part of antenna design. A proper feed method not only considers antenna performance but also satisfies the physical limitations of real application. The methods for feeding microstrip antennas can be divided into two main categories: contacting and non-contacting methods [6].

In the contacting method, as the name implies, the RF signal is fed directly to the radiating patch by a conductive element such as a probe (coaxial feed) or a microstrip line (inset feed or quarter-wavelength transmission line feed). In the non-contacting method, RF power is transferred to the radiating patch through electromagnetic coupling. The coupling can directly connect the patch and the microstrip line (i.e., a proximity-coupled feed) or it can use an aperture slot (i.e., an aperture-coupled feed).

The simplest method is the coaxial (or probe) feed shown in Figure 1.7(a). The inner conductor (pin) of a coaxial connector pierces through the ground plane and substrate layer and is soldered onto the radiating patch, while the outer conductor is connected to the ground plane. The advantage of a coaxial feed is its simplicity in fabrication and the ease with which it accomplishes impedance matching. The major disadvantage of a coaxial feed is that it provides limited bandwidth and requires a bulky structure. The feeding location can be calculated according to previously published formulas [6], [9].

In the quarter-wavelength transmission line feed (also called the direct feed), as the name implies, the RF power is fed directly into the edge of patch through a quarter-wavelength transmission line element between the patch and the microstrip line for impedance matching, as shown in Figure 1.7(b). This occurs because the characteristic impedance of a microstrip line is 50 Ω, but the impedance on the edge of the patch is typically very large, ranging from 300 to 400 Ω. The advantage of a direct feed is its low profile, low cost, easy fabrication, and ease of impedance matching; its major disadvantages are limited bandwidth and extra space requirements due to the quarter-

wavelength transformer. The design process of a quarter-wavelength transformer has been described in previous work [10].

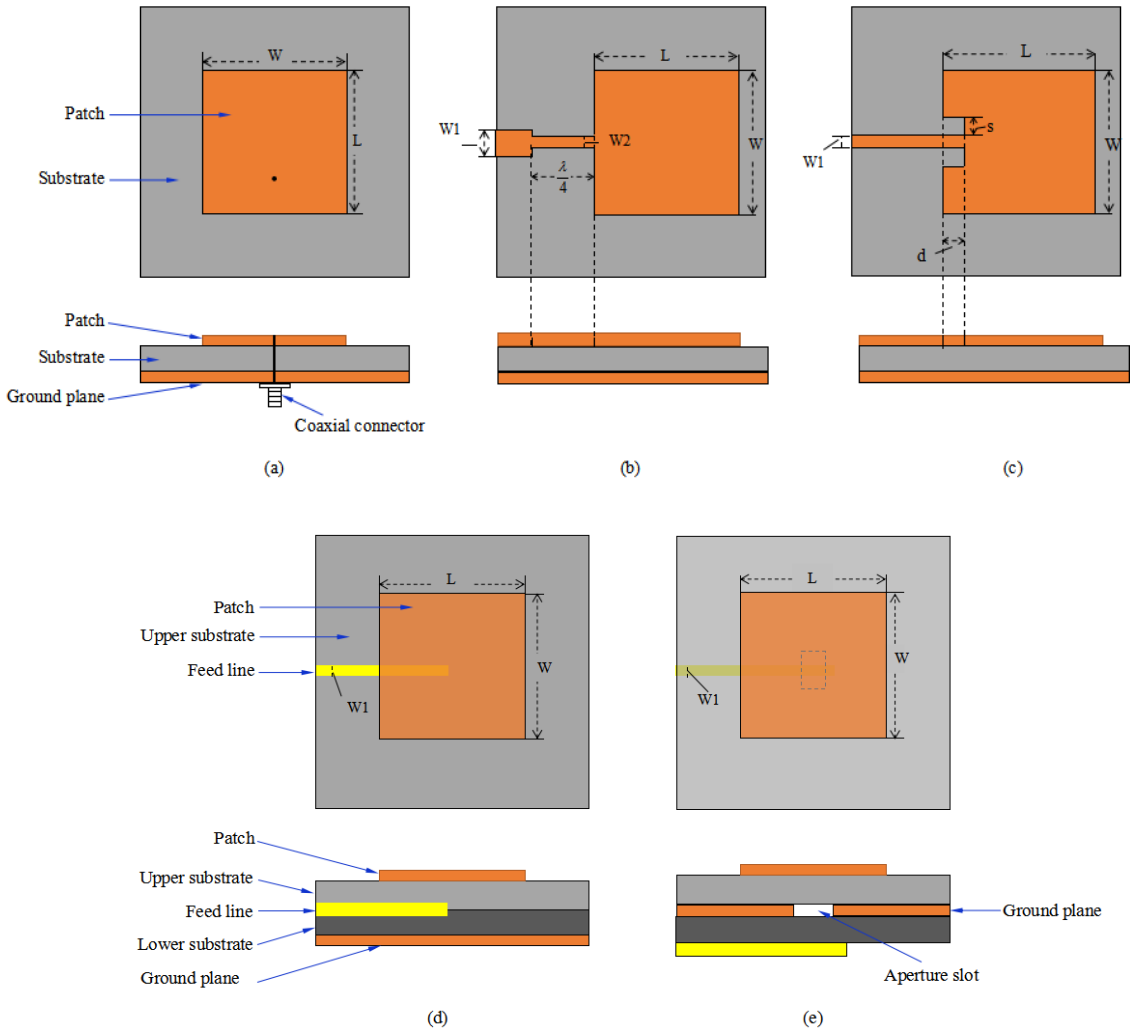

Figure 1.7 (a) Coaxial feed. (b) Quarter-wavelength transmission line feed. (c) Inset feed. (d) Proximity feed. (e) Aperture-coupled feed.

In the inset feed method, the microstrip line is embedded into the radiating patch, approaching the point at which it has the same impedance as the microstrip line, as shown in Figure 1.7(c). Compared to the quarter-wavelength transmission line feed, a major

advantage of the inset feed is the compact size of its feeding structure, which is suitable for microstrip array antennas.

Proximity-coupled feeds are widely used in modern RF systems because they provide very high bandwidth, up to 15 percent. Another advantage of proximity-coupled feeds is that they add an extra degree of freedom to the design, which is very helpful when designing array antennas at higher frequencies [6]. The structure is shown in Figure 1.7(d). The microstrip line is enclosed in two substrate layers, terminating under the patch after a certain length. The RF power is transferred to the patch through electromagnetic coupling between the patch and the microstrip line. The dielectric constants of the two substrate layers can be different to enhance antenna performance [11-13].

Aperture feeds represent another commonly used non-contacting feeding method with advantages such as highly integration, lower interference, and higher bandwidth. The major difference relative to a proximity feed is that a ground plane with an aperture slot is located between the microstrip line and the radiating patch. The RF power is coupled from the transmission line into the patch through the aperture slot, which can be designed with any size or shape for enhanced antenna performance [6]. Because the patch and transmission feed line are separated by the ground plane, the patch substrate (upper substrate) can be made using a lower dielectric constant material to yield better radiation. The feed substrate (lower substrate) can be independently chosen to have a high-dielectric constant material, thus producing tightly coupled fields that do not transmit spurious radiation [14-15]. The major disadvantage of an aperture feed is the complexity of its fabrication, due to its multilayer structure, as shown in Figure 1.7(e).

1.4.3 Half-Wavelength Rectangular/Square Patch Antenna

The half-wavelength rectangular patch antenna is often used to explain the design process of a microstrip antenna. Three critical parameters are involved in the design of a rectangular patch: width W, length L and effective dielectric constant ε_{r_eff}. The patch width is usually chosen to achieve high antenna efficiency [6], [9] and defined as follows:

$$W = \frac{c}{2f}\left(\frac{2}{\varepsilon_r+1}\right)^{1/2} \tag{1.5}$$

Next, the effective dielectric constant of the substrate is given as follows:

$$\varepsilon_{r\_eff} = \frac{\varepsilon_r+1}{2} + \frac{\varepsilon_r-1}{2}\left(1+\frac{10h}{W}\right)^{-1/2} \tag{1.6}$$

With an effective dielectric constant and patch width, the length of the fringing field can be calculated using the following formula:

$$\Delta L = 0.412 \cdot h \cdot \frac{(\varepsilon_{r\_eff}+0.3)\left(0.264+\frac{W}{h}\right)}{(\varepsilon_{r\_eff}-0.258)\left(0.8+\frac{W}{h}\right)} \tag{1.7}$$

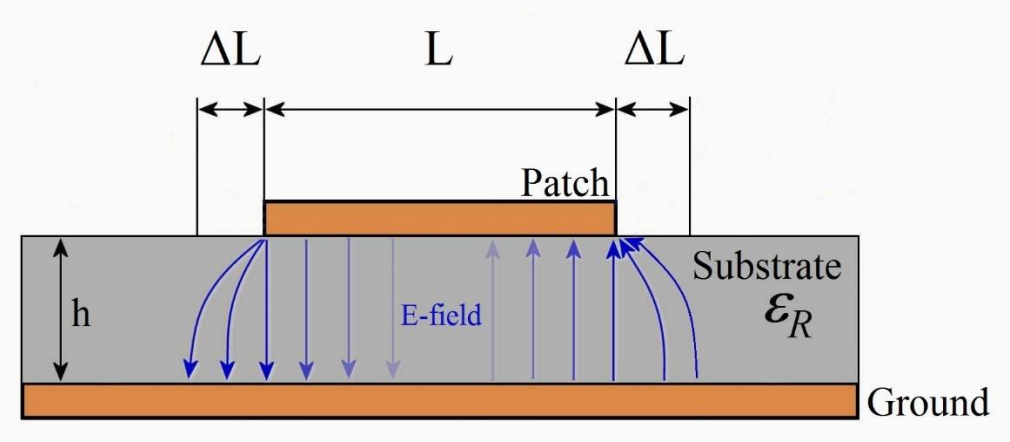

Figure 1.8 Diagram of cutaway view of the patch antenna with E-field.

Fringing field is the extension of electric field out of patch, as shown in figure 1.8. Inside the patch, the electric field resonates in a straightforward manner between the patch and the ground, but at the edge of the patch, the fringing effect makes the electric field closely parallel to the patch, forming the fringing field. Hence, the actual electrical length of the patch is slightly larger than the physical length L. The half-wavelength refers to the electrical length of the patch; thus, the physical length L is given as follows:

$$L = \frac{\lambda_0}{2} \cdot \frac{1}{\sqrt{\varepsilon_{r_{eff}} \cdot \mu_{r_{eff}}}} - 2\Delta L \tag{1.8}$$

where λ_0 is free-space wavelength at resonant frequency.

As introduced in the previous section, the simplest method of exciting a patch antenna involves using a coaxial (probe) feed. The input impedance can be changed by adjusting the location of the feed. Δfed represents the distance from the edge to probe, and the antenna input impedance decreases as the Δfed increases. For half-wavelength rectangular patches, the value of Δfed is given as follows:

$$Z_A(\Delta\text{fed}) = Z_A(\Delta\text{fed} = 0) \cdot \cos^2\left(\pi \cdot {\Delta\text{fed}}/{L}\right), \text{ where } Z_A = 90\frac{{\varepsilon_r}^2}{\varepsilon_r - 1}\left(\frac{L}{W}\right)^2 \tag{1.9}$$

1.4.4 Cavity Model of Microstrip Patch Antennas

There are several methods for analyzing microstrip antennas. The most popular one is the transmission line model, which assumes that the patch is a transmission line or a part of a transmission line. The transmission line model is the simplest way to analyze microstrip antennas and relies on physical insight. However, it is not suitable for a patch

due to the patch's nonuniform shape, as well as the model's low accuracy and difficulty with simulating coupling.

The cavity model assumes that the patch is a dielectric-loaded cavity with a perfect electric conductor (PEC) at the top and bottom and a perfect magnetic conductor (PMC) in the substrate around the patch. Compared to the transmission line model, the cavity model is more complex, but provides more accurate results and makes greater physical sense [16]. In this section, a microstrip half-wavelength rectangular patch antenna is analyzed using the cavity model.

Once a rectangular patch is excited, the input source is generally a certain modulated sinusoidal voltage signal, creating an oscillation in the electric field between the patch and the ground panel along with the length of the patch (with length L being the half-wavelength in the substrate). As a result, a positive charge is concentrated on one side of the patch, while a negative charge is concentrated on the other side. This charge distribution induces two forces in the cavity. As shown in Figure 1.9, the first is the attractive force between the opposite charges on the bottom of the patch and the ground plane surface.

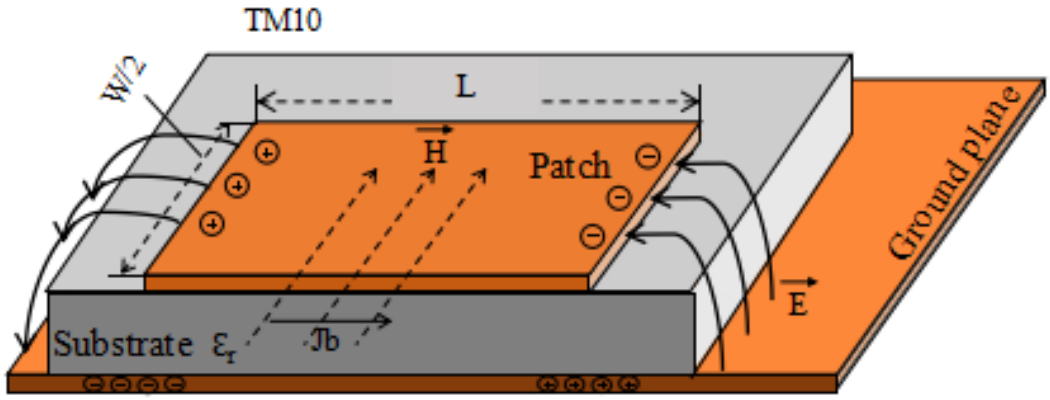

Figure 1.9 A 3D view of rectangular patch antenna.

This attraction force concentrates the patch charge at the bottom of the patch. The second force introduce is the repulsive force between like charges on the bottom of the patch. This force pushes some of the charges around the edge of the patch to the top surface. If the dielectric substrate is very thin, the second force is negligible, and the first force is dominant. Thus, most of the current flow on the bottom side of the patch and on the top and sides of the patch is close to zero. Therefore, the tangential component of the magnetic field is nearly zero close to the edge of the patch. Based on this result, because the height of the substrate h is much smaller than the wavelength, the wall between the patch edge and ground plane can be assumed to be a PMC. Therefore, only transverse magnetic (TM) modes inside the cavity are considered [17-18].

Considering the microstrip rectangular patch antenna shown in Figure 1.10, the center of the patch can place at the origin of a rectangular coordinate system, assuming that

the antenna is propagating in the z direction, and feeding point locates on y-axis. Based on the cavity model, the dominant mode of this rectangular patch antenna is TM_{10}.

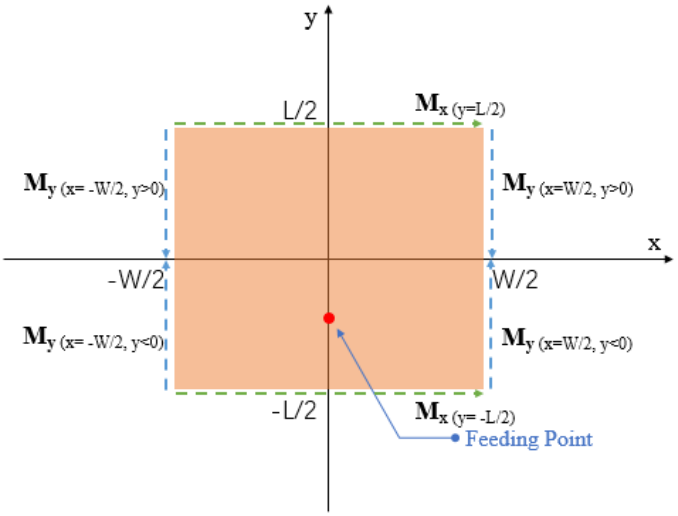

Figure 1.10 Diagram of cavity model in a probe feed rectangular patch antenna.

Because the cavity model assumes that the field distribution under the patch antenna is the same as that in a cavity, the radiated power can be considered as leakage energy from the cavity's sidewalls. The field theorem indicates that the magnetic current (theoretically, although this may not exist in practice) is a contribution of the electric field.

$\overrightarrow{\boldsymbol{M_s}} = \hat{\boldsymbol{E}}$ x $\hat{\boldsymbol{n}}$, where n is the direction normal to the sidewall. (1.10)

thus,

$$\overrightarrow{\boldsymbol{M_y}} = E_z \cdot \pm\hat{\boldsymbol{z}} \times \hat{\boldsymbol{x}}$$

$$= \pm E_0 \cdot \cos\left({}^{n\pi y}/_{L}\right)\hat{\boldsymbol{y}} \quad for\ x = \pm\frac{w}{2}, -\hat{\boldsymbol{z}}\ if\ y > 0;\ +\hat{\boldsymbol{z}}\ if\ y < 0 \qquad (1.11)$$

$$\overrightarrow{\boldsymbol{M_x}} = \pm E_z \cdot \hat{\boldsymbol{z}} \times \pm\hat{\boldsymbol{y}}$$

$$= E_0 \cdot \cos\left({}^{m\pi x}/_{W}\right)\hat{\boldsymbol{x}} \quad for\ y = \pm L/2 \tag{1.12}$$

Because the electric field is sinusoidally distributed between the patch and the ground along the y-axis, the positive and negative portions of the magnetic current on edge x (x = +W/2) cancel, and the same situation occurs for edge x = -W/2. Thus, the total magnetic current in the y direction $\overrightarrow{\boldsymbol{M_y}}$ is zero. On edge y = ±L/2, because the electrical field distribution and the normal direction of the sidewalls are always opposite, the magnetic current is always the same. The magnetic current is given as follows:

$$\overrightarrow{\boldsymbol{M_x}} = \hat{\boldsymbol{E}} \text{ x } \hat{\boldsymbol{n}} = E_z \cdot \hat{\boldsymbol{x}}, \tag{1.13}$$

which indicates the source of the radiated energy. Because the magnetic current is conceptual, it does not physically exist.

The ψ function for wave equation is given as follows:

$$\psi_{mn} = \frac{\chi_{mn}}{\sqrt{WL}}\cos(k_m x)\cos(k_n y), \text{ with } \chi_e = \begin{cases} 1, & m = 0\ and\ n = 0; \\ \sqrt{2}, & m = 0\ or\ n = 0; \\ 2, & m \neq 0\ and\ n \neq 0; \end{cases} \tag{1.14}$$

thus,

$$E_z = \psi_{01} = \sqrt{\frac{2}{WL}} \cdot \cos\left(\frac{\pi}{L}y\right) \tag{1.15}$$

The electrical vector potential $\vec{\boldsymbol{F}}$ can be derived from magnetic current as follows:

$$\vec{\boldsymbol{F}}(\vec{\boldsymbol{r}}) = \iiint \overrightarrow{\boldsymbol{M}}(r')\, e^{j\vec{k}\vec{r'}} dv' \text{ , where } r' \text{ indicates the source.} \tag{1.16}$$

thus, at edge y = L/2,

$$\vec{\boldsymbol{F}}(\vec{\boldsymbol{r}}) = \sqrt{\frac{2}{WL}} \int_{-\frac{W}{2}}^{+\frac{W}{2}} e^{jk_x x'} e^{jk_y \frac{L}{2}} dx' \tag{1.17}$$

$$\vec{\boldsymbol{F}}(\vec{\boldsymbol{r}}) = \sqrt{\frac{2}{WL}}\, e^{jk_y \frac{L}{2}}\, \frac{1}{jk_x} \left(e^{jk_x \frac{W}{2}} - e^{-jk_x \frac{W}{2}} \right) \tag{1.18}$$

$$\vec{\boldsymbol{F}}(\vec{\boldsymbol{r}}) = 2\sqrt{\frac{2}{WL}}\, e^{jk_y \frac{L}{2}}\, \frac{\sin\left(k_x \frac{W}{2}\right)}{k_x} \tag{1.19}$$

Assuming that, $\phi_x = k_x \frac{W}{2}$ and $\phi_y = k_y \frac{L}{2}$, $\vec{\boldsymbol{F}}(\vec{\boldsymbol{r}})$ can be simplified as follows:

$$\vec{\boldsymbol{F}}(\vec{\boldsymbol{r}}) = 2\sqrt{\frac{2W}{L}} \frac{\sin(\phi_x)}{\phi_x} e^{jk_y \frac{L}{2}} \tag{1.20}$$

Similarly, at edge y = -L/2,

$$\vec{\boldsymbol{F}}(\vec{\boldsymbol{r}}) = 2\sqrt{\frac{2W}{L}} \frac{\sin(\phi_x)}{\phi_x} e^{-jk_y \frac{L}{2}} \tag{1.21}$$

thus, the total $\vec{\boldsymbol{F}}(\vec{\boldsymbol{r}})$ is as follows:

$$\vec{\boldsymbol{F}}(\vec{\boldsymbol{r}}) = 2\sqrt{\frac{2W}{L}} \frac{\sin(\phi_x)}{\phi_x} e^{jk_y \frac{L}{2}} + 2\sqrt{\frac{2W}{L}} \frac{\sin(\phi_x)}{\phi_x} e^{-jk_y \frac{L}{2}} = 4\sqrt{\frac{2W}{L}} \frac{\sin(\phi_x)}{\phi_x} \cos\left(\phi_y\right) \tag{1.22}$$

With vector potential $\vec{\boldsymbol{F}}(\vec{\boldsymbol{r}})$, E_θ and E_ϕ can be derived from the solution of Maxwell's equations as follows:

$$\vec{\boldsymbol{E}} = -\nabla \times \vec{\boldsymbol{F}} + \frac{1}{j\omega\varepsilon}\left(\nabla \times \nabla \times \vec{\boldsymbol{A}} - \vec{\boldsymbol{J}}\right), \text{ where } \vec{\boldsymbol{A}} \text{ and } \vec{\boldsymbol{J}} \text{ are zero} \tag{1.23}$$

$$E_\theta = -jk\eta\overrightarrow{\boldsymbol{A_\theta}} - jk\overrightarrow{\boldsymbol{F_\phi}} = -jk\overrightarrow{\boldsymbol{F_\phi}} \tag{1.24}$$

$$E_\phi = -jk\eta\overrightarrow{\boldsymbol{A_\phi}} + jk\overrightarrow{\boldsymbol{F_\theta}} = jk\overrightarrow{\boldsymbol{F_\theta}} \tag{1.25}$$

and far-field proximation yields the following expressions:

$$E_\theta = \frac{e^{-jkr}}{4\pi r} jkh\left(F_x \sin\phi - F_y \cos\phi\right) \tag{1.26}$$

$$E_\phi = -\frac{e^{-jkr}}{4\pi r} jkh\left(F_x \cos\phi + F_y \sin\phi\right)\cos\theta \tag{1.27}$$

When the rectangular patch antenna is fed by a coaxial cable, many waves are excited, which results in several possible field representations inside the cavity. The electric field inside the patch cavity can be expressed in various models of the cavity as follows:

$$E_z = \sum_m \sum_n A_{mn}\, \psi_{mn}(x, y) \tag{1.28}$$

where A_{mn} is the amplitude coefficient corresponding to the electrical field mode vector or eigenfunction ψ_{mn}. The eigenfunction ψ_{mn} must satisfy the homogeneous wave equation, boundary conditions and normalization conditions as follows:

$$\left.\frac{\partial\psi_{mn}}{\partial x}\right|_{x=0} = \left.\frac{\partial\psi_{mn}}{\partial x}\right|_{x=L} = 0 \tag{1.29}$$

$$\left.\frac{\partial\psi_{mn}}{\partial y}\right|_{y=0} = \left.\frac{\partial\psi_{mn}}{\partial y}\right|_{y=W} = 0 \tag{1.30}$$

$$(\nabla^2 + \mathrm{k}_{mn}^2)\,\psi_m = 0 \tag{1.31}$$

$$\left(\frac{\partial^2}{\partial x^2} + \frac{\partial^2}{\partial y^2} + \mathrm{k}_{mn}^2\right)\psi_{mn} = 0 \tag{1.32}$$

separation of variable, ψ_m can be expressed as follows:

$$\psi_m = [A_1 \cos(k_x x) + B_1 \sin(k_x x)]\left[A_2 \cos\left(k_y y\right) + B_2 \sin(k_y y)\right][A_3 \cos(k_z z) + B_3 \sin(k_z z)] \quad (1.33)$$

where k_x, k_y and k_z are the wavenumbers along the x, y, and z directions.

The electrical and magnetic fields within the cavity are related to the vector potential, which can be given as follows:

$$E_x = -j\frac{1}{\omega\mu\epsilon}\left(\frac{\partial^2\psi_m}{\partial x \partial z}\right), H_x = -\frac{1}{\mu}\frac{\partial\psi_m}{\partial y} \quad (1.34)$$

$$E_y = -j\frac{1}{\omega\mu\epsilon}\left(\frac{\partial^2\psi_m}{\partial x \partial y}\right), H_y = \frac{1}{\mu}\frac{\partial\psi_m}{\partial z} \quad (1.35)$$

$$E_z = -j\frac{1}{\omega\mu\epsilon}\left(\frac{\partial^2}{\partial z^2} + k^2\right)\psi_m \quad (1.36)$$

according to the following boundary conditions:

$$E_y(0 \le x' \le W, 0 \le y' \le L, z' = 0) = E_y(0 \le x' \le W, 0 \le y' \le L, z' = h) = 0 \quad (1.37)$$

$$H_y(x' = 0, 0 \le y' \le L, 0 \le z' \le h) = H_y(x' = W, 0 \le y' \le L, 0 \le z' \le h) = 0 \quad (1.38)$$

$$H_z(0 \le x' \le W, y' = 0, \le z' \le h) = H_z(0 \le x' \le W, y' = L, 0 \le z' \le h) = 0 \quad (1.39)$$

The primed coordinates $x', y' \; and \; z'$ represent the fields inside the cavity. By applying the boundary condition $B_1 = B_2 = B_3 = 0$, and the following parameters:

$$k_x = \frac{m\pi}{W} \, , m = 0,1,2, ... \tag{1.40}$$

$$k_y = \frac{n\pi}{L} \, , n = 0,1,2, ... \tag{1.41}$$

$$k_z = \frac{p\pi}{h} \, , h = 0,1,2, ... \tag{1.42}$$

Therefore, the final form of the vector potential within the cavity is:

$$\psi_m = A_{mn} \cos(k_x x') \cos\left(k_y y'\right) \cos(k_z z'), \tag{1.43}$$

where A_{mn} represents the amplitude coefficients of each mode.

For a rectangular patch, $k_z = 0$ and the vector potential is given as follows:

$$\psi_m(x, y) = \sqrt{\frac{\epsilon_m \epsilon_n}{LW}} \cos\left(\frac{m\pi}{W} x\right) \cos\left(\frac{n\pi}{L} y\right) \tag{1.44}$$

and

$$k_{mn} = \sqrt{\left(\frac{m\pi}{W}\right)^2 + \left(\frac{n\pi}{L}\right)^2} \tag{1.45}$$

The amplitude coefficients A_{mn} are determined by substituting equation (2.42) into equation (2.37). Next, both sides of equation (2.37) are multiplied by $\psi_m{}^*$ and integrated over the area of the patch. Therefore, A_{mn} can be expressed as follows:

$$A_{mn} = \frac{j\omega\mu_o}{k_A^2 - k_{mn}^2} \iint J_z \, \psi_m{}^* dx dy \tag{1.46}$$

Next, the coaxial probe feed can be modeled using Huygen's principle, which involves current flowing along the center conductor from the bottom to the top. The probe has a diameter d where the conductor pin passes through it and is connected to the patch [19].

$$A_{mn} = \frac{j\omega\mu_o I_o}{k_A^2 - k_{mn}^2} \sqrt{\frac{\epsilon_m \epsilon_n}{LW}} cos\left(\frac{m\pi}{W} x_o\right) cos\left(\frac{n\pi}{L} y_o\right) G_{mn} \tag{1.47}$$

$$G_{mn} = sinc\left(\frac{n\pi d}{2L}\right) \tag{1.48}$$

Thus, equation (1.46) can be written as follows:

$$A_{mn} = \frac{j\omega\mu_o I_o}{k_A^2 - k_{mn}^2} \sqrt{\frac{\epsilon_m \epsilon_n}{LW}} cos\left(\frac{m\pi}{W} x_o\right) cos\left(\frac{n\pi}{L} y_o\right) sinc\left(\frac{n\pi d}{2W}\right) \tag{1.49}$$

Therefore, E_z can be expressed as follows:

$$E_z(x,y) = j\omega\mu_o I_o \sum_m \sum_n \frac{\psi_m(x,y)\psi_m(x_o,y_o)}{k_A^2 - k_{mn}^2} sinc\left(\frac{n\pi d}{2W}\right) \tag{1.50}$$

Because the input impedance inside the cavity is defined as follows:

$$Z_{in} = \frac{V_{in}}{I_o} \tag{1.51}$$

where $V_{in} = -E_z(x_o, y_o) * h$ at the feed point, and V_{in} can be written as:

$$V_{in} = -j\omega\mu_o h I_o \sum_m \sum_n \frac{{\psi_m}^2(x_o,y_o)}{k_A^2 - k_{mn}^2} sinc\left(\frac{n\pi d}{2W}\right) \tag{1.52}$$

Equation (1.50) can be rewritten from equation (1.51) as follows:

$$Z_{in} = -j\omega\mu_o h \sum_m \sum_n \frac{{\psi_m}^2(x_o, y_o)}{k_A^2 - k_{mn}^2} sinc\left(\frac{n\pi d}{2W}\right) \quad (1.53)$$

Assume that $sinc\left(\frac{n\pi d}{2W}\right) = \frac{\sin\left(\frac{m\pi d}{2W}\right)}{\left(\frac{m\pi d}{2W}\right)} = 1$; thus, from equation (1.52), the input impedance is as follows:

$$Z_{in} = -j\omega\mu_o h \sum_m \sum_n \frac{{\psi_m}^2(x_o, y_o)}{k_A^2 - k_{mn}^2} \quad (1.54)$$

For a coaxial probe feed microstrip antenna, the feed is modeled separately, and its reactance is calculated and added to the input impedance of the patch antenna. The coaxial feeding structure is modeled as a thin strip of finite width with a uniformly distributed electric current flowing vertically from the ground plan to the patch. The probe reactance can be expressed as an inductance with no resonant models of the cavity. For a rectangular patch antenna, the probe reactance can be expressed as follows:

$$X_p = -\frac{\eta kh}{2\pi}\left[ln\left(\frac{kd}{4}\right) + 0.577\right] \quad (1.55)$$

where

$$k_A^2 = k_o^2 \epsilon_{reff}\left(1 - \frac{j}{Q_t}\right) \quad (1.56)$$

$$k_{mn}^2 = \left(\frac{m\pi}{W}\right)^2 + \left(\frac{n\pi}{L}\right)^2 \quad (1.57)$$

$$\eta = \eta_o \sqrt{\frac{\mu_r}{\epsilon_r}} \quad (1.58)$$

$$k = \frac{\omega\sqrt{\epsilon_r \mu_r}}{c} \quad (1.59)$$

CHAPTER 2

CIRCULARLY POLARIZED MICROSTRIP PATCH ANTENNAS

There are multiple types of antennas with circular polarization. The helix and cloverleaf are the most famous circularly polarized (CP) wire antennas (see Figure 2.1(a) and (b)). The helix antenna, also called the helical antenna, is a spirally shaped wire antenna with a large ground panel. It provides high gain (approximately 10-15 dB) with an endfire radiation pattern. The cloverleaf antenna has a donut-shaped radiation pattern similar to a dipole antenna with circular polarization [20-21]. The helix antenna has good circular polarization with a directional radiation pattern, whereas the cloverleaf antenna has fairly good circular polarization with an almost omni-directional radiation pattern. However, the bulky structure of these antennas makes them inappropriate for compact mobile devices and is difficult to implement in an array.

Figure 2.1 (a) A 5.8 GHz helix antenna. (b) A 5.8 GHz cloverleaf antenna.

Hence, CP microstrip antennas represent an attractive solution that combines high performance and compact size. As described in Chapter 1, to produce a wave in circular polarization, an antenna should generate two orthogonal electrical field components with equal magnitudes and a 90° phase difference.

2.1 Circularly Polarized Microstrip Patch Antennas

2.1.1 Dual feed CP microstrip antennas

In conventional design, a CP microstrip antenna requires two inputs to excite two orthogonal patch modes with quadrature phasing and equal magnitude. The two feed locations used to excite the two orthogonal patch modes are shown in Figure 2.2. Usually, the two ports are fed physically from two sources that have equal magnitude and are 90º out of phase, or from the help of an external polarizer, such as a quadrature hybrid T-junction power divider. Such a two-feed mechanism results in a bulky and expensive structure. Additionally, it is difficult to ensure that the magnitude of the two feeding ports is exactly the same, which impacts the overall performance of the AR [22-24].

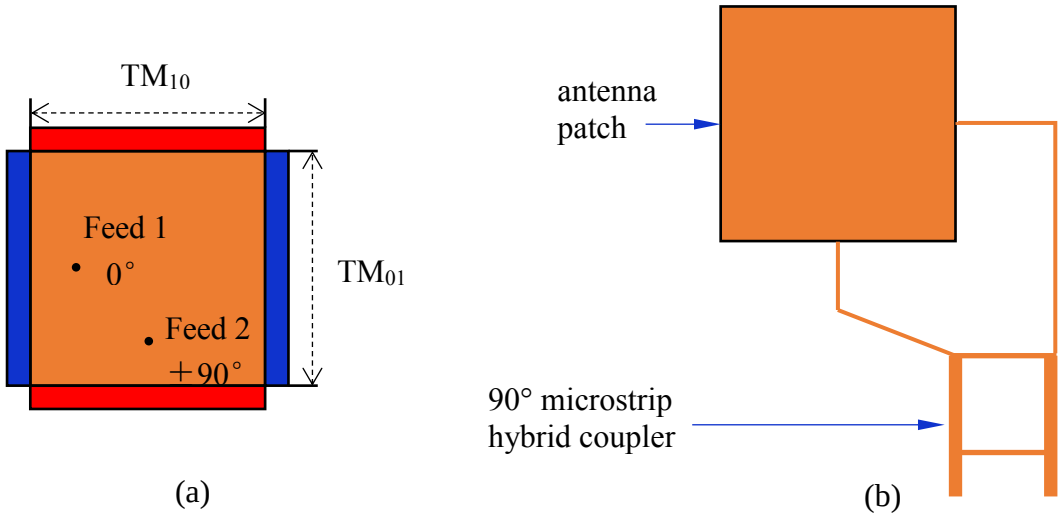

Figure 2.2 (a) Typical dual-fed circularly polarized patch antennas. (b) Typical dual-fed circularly polarized patch antennas from a single port.

2.1.2 Single-feed CP microstrip antennas

One simple choice is to construct a two-feed structure with a single microstrip line, as shown in Figure 2.2(b). Because of feeding mismatch, a typical antenna with this structure has a 6-dB AR bandwidth of approximately 3% with a minimum AR of 1 dB [24]. However, such an antenna will not perform adequately in some applications.

Other SF CP microstrip antennas have been proposed to improve antenna performance. Truncated corner, square patch with a diagonal slot, and diagonal-fed nearly square antennas are common configurations in the industry due to their simple structures [25-30], [35-37].

Using these three configurations, a 0.2 dB minimum AR can easily be achieved. However, their 6-dB AR bandwidths are reduced to nearly 0.9-1%. Nevertheless, SF CP

microstrip antennas are widely used for global positioning systems (GPSs), since they feature easy fabrication, low cost, and wide beamwidth.

Compared to dual feed circularly polarized patch antennas, SF CP patch antennas have a narrow AR bandwidth [31-34]. However, in recent decades, several bandwidth-enhancement techniques have been successfully implemented for SF CP antennas. Because of these improvements in bandwidth, SF CP patch antennas are more competitive, especially in array applications.

The performances of the antennas discussed above are summarized in Table 2.1.

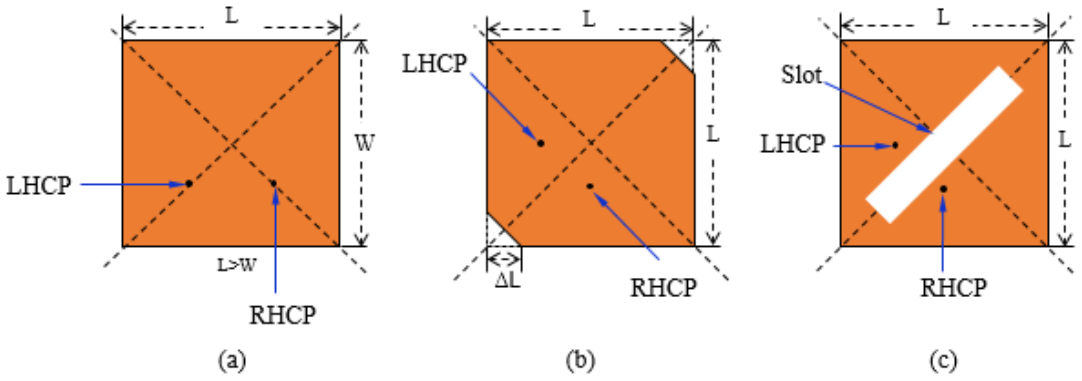

Figure 2.3 Three typical topologies of single fed circularly polarized patch antennas: a. diagonal-fed nearly square patch antenna; b. truncated corners square patch antenna; c. diagonal slot squa1re patch antenna.

Table 2.1 Summary of AR performance of circular polarized microstrip patch antennas.

	Microstrip dual-feeds	Diagonal-fed nearly square	Truncated-corners	Diagonal slot
Minimum AR	1 dB	0.25 dB	0 dB	0.2 dB
6-dB AR bandwidth	>3%	0.67%	0.92%	1.2%

2.2 Proposed Single-Feed Circularly Polarized Patch Antenna

2.2.1 Design methodology

In this study, we introduce a new configuration of a compact CP microstrip antenna with a single feed. The structure is similar to a regular microstrip antenna and the design procedure is relatively simple. The basic operational mechanism for CP radiation is based on a small aperture in the top radiating patch [38-39]. Proper arrangement of the aperture holes will produce two orthogonal degenerate modes, with phases separated by 90° but equal magnitudes, resulting in excellent CP radiation. In this case, the feed location determines not only the input impedance but also the relative magnitudes of the two normal modes.

Here, we assume that the substrate thickness is much smaller than the wavelength and that there is no field variation in the direction perpendicular to the patch. Two small circular apertures are placed along the y-axis, while the feed is located near the diagonal line connecting two opposite corners. The feed excites two degenerate modes, TM_{10} and TM_{01}. For the TM_{10} mode, the holes act as induced magnetic dipoles, because the small apertures are located where the magnetic field is at a maximum, but the electrical field is vanishing. On the other hand, for the TM_{10} mode, the holes behave as both electrical and magnetic dipoles because of the presence of both electrical and magnetic fields at the hole locations. As the holes move closer to the patch edges, the equivalent electric dipole moments at the apertures dominate the magnetic dipole moments, because the magnetic field decreases towards the patch edges [39]. Since the field excitation due to a magnetic dipole is 90° out of phase with that due to an electric dipole, the degenerate modes excited

by the feed have different boundary conditions. Once the hole locations are properly chosen, the apertures impose boundary conditions that produce two modal excitations with a phase difference of 90° [25, 26].

Because the two degenerate modes have different boundary conditions, the feed at the diagonal line results in close but not exactly equal magnitudes for the two modes; it is necessary to adjust the relative field magnitude of one mode relative to the other by shifting the feed location. For example, as the feed moves towards one edge with a fixed value of x, the cavity model shows that the field magnitude of TM_{01} will increase relative to that of TM_{10}. A relatively minor shift is required to yield two degenerate modes with equal magnitudes.

The holes must be large enough for the apertures to exert a sufficient influence on the modal excitations, resulting in the required phase shift of 90° for CP radiation. However, overly large holes will not act as ideal 90° phase shifters, because the 90° phase shift is based on a small-hole approximation [40]. To increase the effect of the aperture holes while minimizing the detrimental effects of large aperture size, two holes are symmetrically placed, as shown in Figure 2.4. Those two holes will influence the modal excitations equally

2.2.2 HFSS simulation and optimization

High-frequency electromagnetic field simulation (HFSS) is commonly used in resonant antenna simulation and was selected for the simulation work in this dissertation. The design work and parameters are shown in Figure 2.4. The substrate is Rogers RO

4003C (design ϵ_r = 3.55 and dissipation factor = 0.0027) with a thickness of 60 mils (1.524 mm). Copper is used for the patch and ground (σ = 5.8 x 10^7 s/m), with a thickness of 35 micrometers. The initial antenna dimensions are shown in Table 2.1, as calculated by cavity mode analysis. L represents the length and width of the square patch, and two circular slots with a radius of 3 mm are placed along the y-axis with a 10.86 mm offset to the center point of the patch. The feeding location is placed on the diagonal line in the second quadrant, with the offset distances to the x- and y-axes represented by Uf and Vf, respectively.

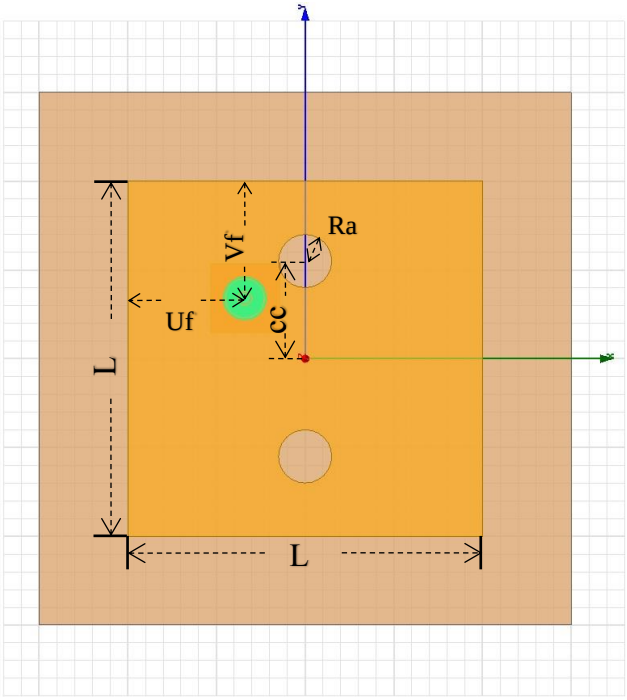

Figure 2.4 Proposed single-feed CP microstrip patch antenna.

Table 2.2 Final optimized design parameters of sub-2GHz single feed CP patch antenna.

Items	Parameter name	Value (mm)
Length of square patch	L	40
Radius of circle slot	Ra	3
Distance to patch center	CC	10.86
Feeding point in x-axis	Uf	5.76
Feeding point in y-axis	Vf	5.76

The simulation results show that this initial designed antenna does not perform well. As indicated in the previous section, circular polarization results from the combined effects of three parameters: feed location, the radius of the circular slots, and the slot offset distance. HFSS supports parametric optimization analysis to determine the proper value for each parameter. Figure 2.5 presents S11 on a logarithmic scale and on a Smith chart. The two dips in Figure 2.5 S11 and the kink near the center of the trace in the Smith chart indicate the presence of two nearly degenerate modes excited within the antenna cavity.

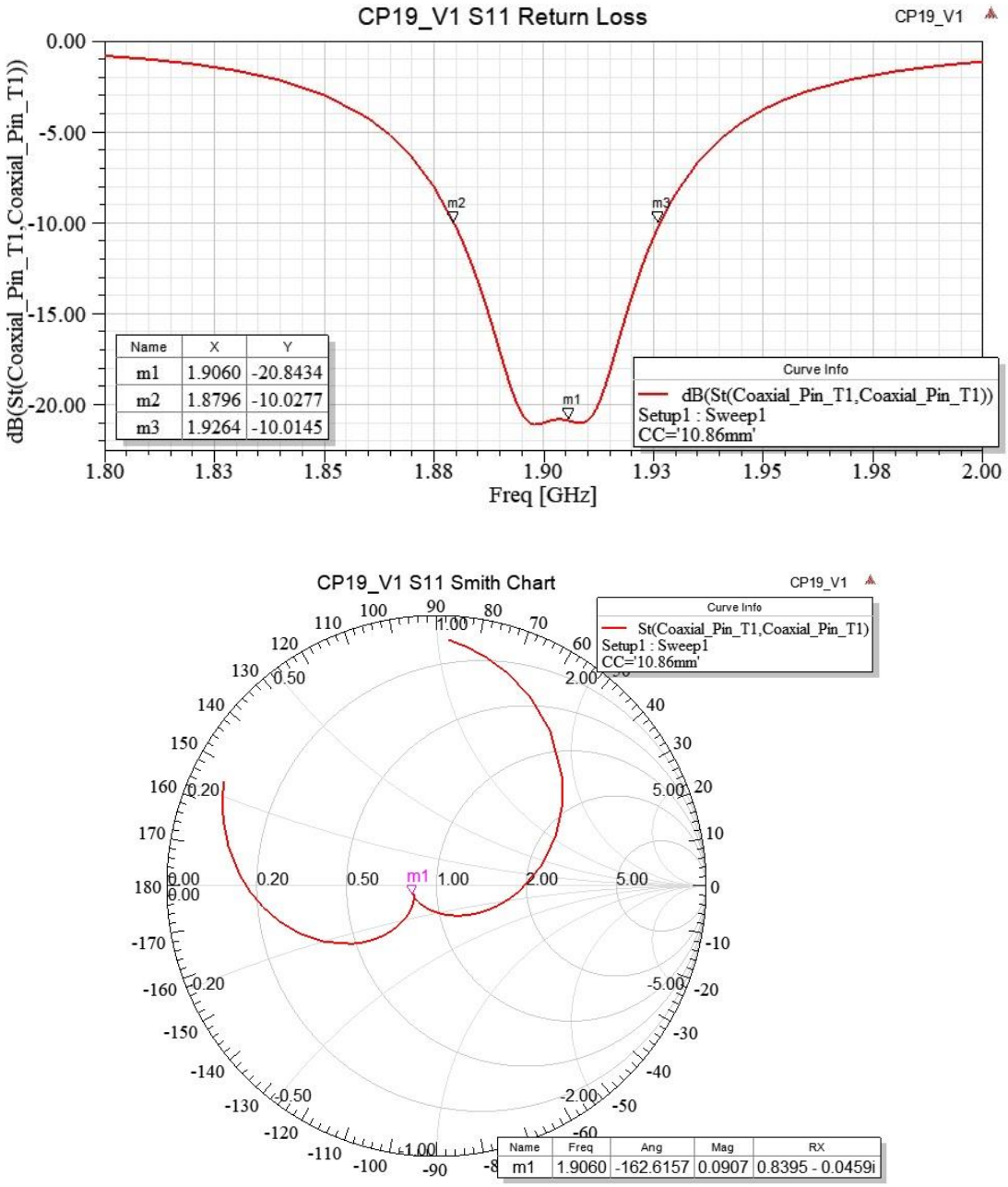

Figure 2.5 Simulated S11 return loss and Smith chart of optimized design.

The distance between the square patch center and the coupling circular slots varies from 8 mm to 15 mm. The S11 has a center frequency at 1.903 GHz with an approximately

-20 dB return loss and a 2.46% 10-dB bandwidth (46.8 MHz), which are similar to those of a normal SF linearly polarized rectangular patch antenna.

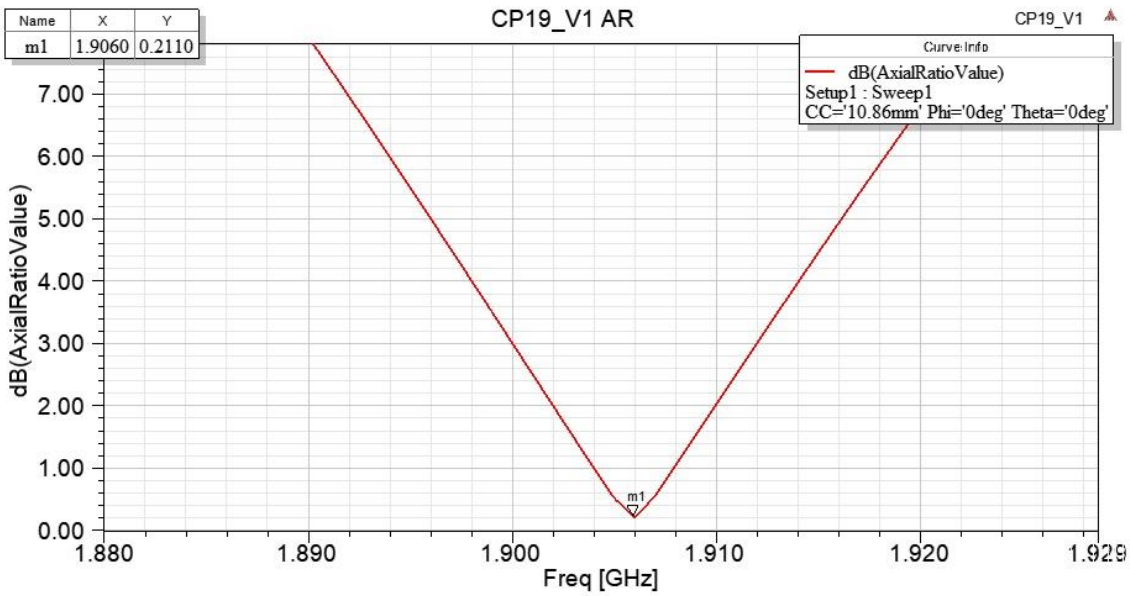

Figure 2.6 The simulated axial ratio (AR) of proposed antenna.

The performance of the designed CP can be evaluated in HPSS by checking the complex magnitude plot of the electrical field distribution on the patch. HFSS defines the complex magnitude plot of an electric field as the result of the complex multiplication of conjugated values [EE*]. Hence, the plot shows the maximum amplitude of the E-field at each point, and this value is phase- (or time-) independent. Because the electric field is sinusoidally distributed, its maximum magnitude occurs on the edges of the patch, and zero E-field is produced in the center of the patch. Thus, for a linearly polarized patch, the complex magnitude of the E-field should be linearly distributed, with a string-shaped region on the patch where the amplitude is close to zero. If the patch produces a CP wave,

the sinusoidally distributed E-field should rotate around the center of patch clockwise or counterclockwise, resulting in a low, circular electric field region relative to the linearly polarized patch, as shown in Figure 2.7. The dark blue region in the center of the figure has a perfectly circular shape, which indicates that the antenna is producing a good circular polarization wave.

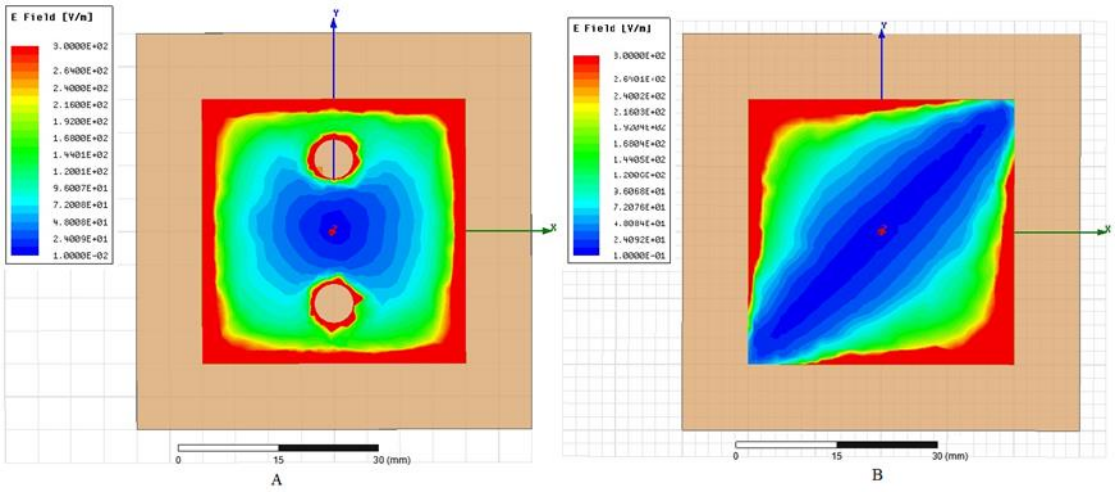

Figure 2.7 Complex magnitude of the electric field on the antenna patch (a) Proposed circularly polarized patch. (b) Linearly polarized diagonal-fed patch.

Figure 2.6 shows that the simulation has a nearly perfect AR of approximately 0.21 dB at 1.906 GHz, yielding a 1.62% (31 MHz) 6-dB and a 0.73% (14 MHz) 3-dB AR bandwidth. The feeding location is along a diagonal line with a 5.76 mm offset from the center of the patch. The two coupling circular slots are placed along the centerline, with 10.86 mm to the antenna patch's center. The 3D radiation pattern is shown in Figure 2.8, indicating a 5.83 dBic RHCP gain with a wide beam width up to 92°.

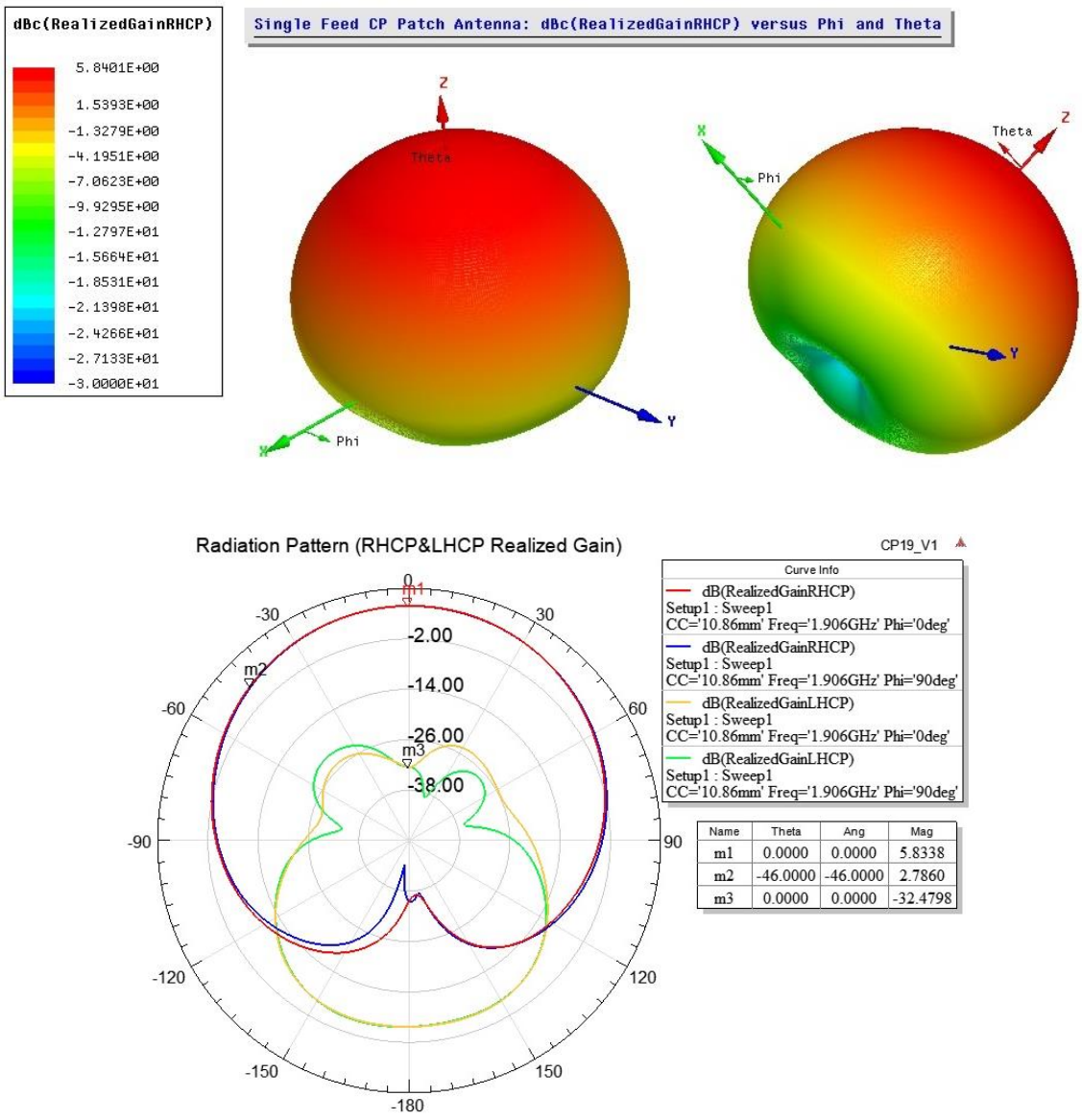

Figure 2.8 Simulated radiation pattern of 3D view and Phi=0º/90º cuts with LHCP.

2.2.3 Measurement Results

The fabrication of all proposed antennas, which was based on simulation parameters, occurred in the Antenna Fabrication Lab at the Lyle School of Engineering, SMU, using an LPKF ProtoMat M60 milling machine (Figure 2.9). The milling machine

was connected to a computer and controlled by the Board Master program run on a Windows system, with a board file imported into the program. In addition to Board Master, the board file was modified using Circuit Cam software to transfer the antenna design from AutoCAD into Board Master format before the milling operation.

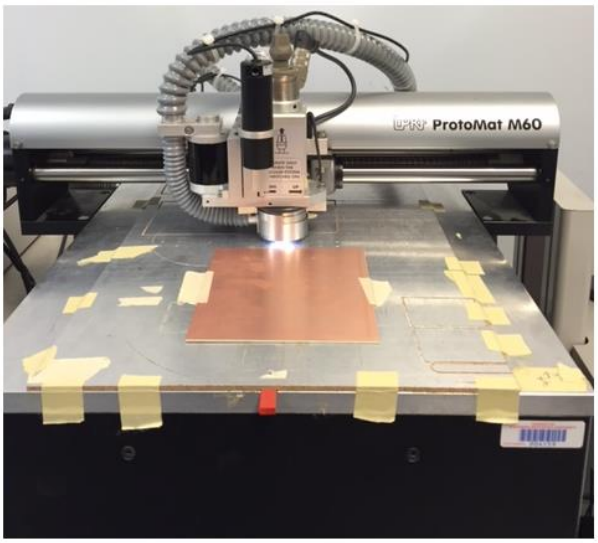

Figure 2.9 The LPKF ProtoMat M60 milling machine in antenna fabrication lab.

Compared to the traditional chemical erosion process, using a milling machine is a simple, low-cost, fast, efficient, and environmentally friendly method of fabricating a microstrip antenna, even though using a milling machine can lower the fabricating accuracy, creating metal burrs and strain on the antenna patch, and over-milling into the substrate, making it unsuitable for multilayer structures.

The fabricated antenna was first used to measure the impedance-matching issue. The antenna was connected to a calibrated professional network analyzer to measure S11, known as the return loss or reflective coefficient. Figure 2.10 shows the results; the

measured data was not consistent with the simulation as usually seen in microstrip antennas. The two concave areas in the return loss plot indicate that two orthogonal modes were excited on different resonant frequencies. The twisting trace in the Smith chart confirms this result; in general, the best AR occurs at the tip of the kink.

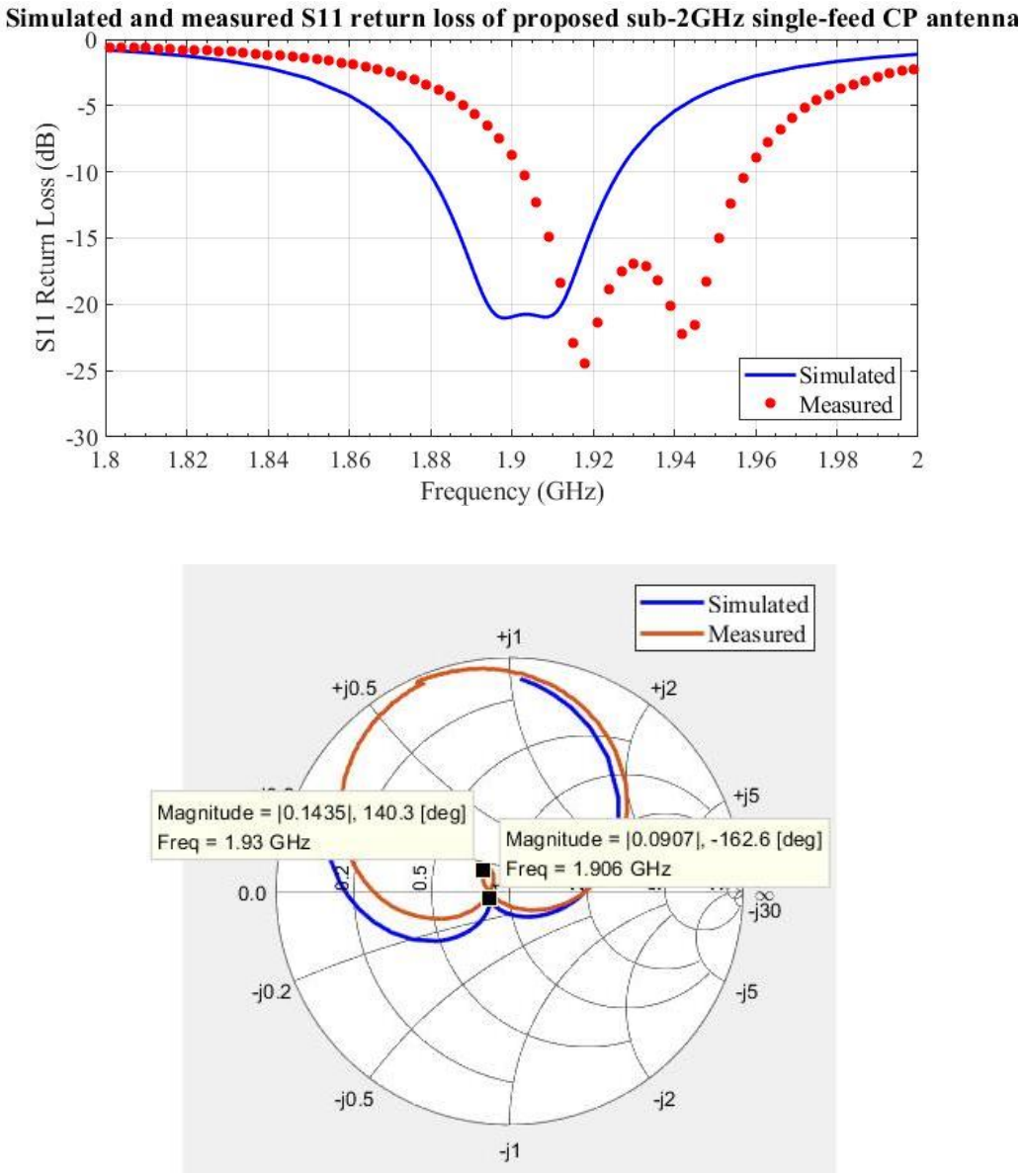

Figure 2.10 Measured and simulated S11 return loss and reflective coefficient.

The measurement work was conducted in the SMU antenna anechoic chamber with an Allwave antenna measurement system (Figure 2.11); a direct test was conducted using a far-field scan with the right-hand polarization option selected. The system uses the gain-compare method to measure the antenna under test (AUT); thus, a standard gain horn (SGH) in the proper frequency range was selected and measured as the reference. The software automatically processes the collected data and reports it to the user.

Figure 2.11 SMU antenna anechoic chamber with Allwave antenna measurement system.

The measured max peak gain is 5.7 dB with a directivity of 6.21 dB at 1.931 GHz, yielding a 88.97% antenna efficiency. Figure 2.12 shows the 2-cut co-pol/x-pol radiation gain pattern in a 2D polar plot with 0º and 90º phi angles. The pattern is similar to that of a regular rectangular microstrip patch antenna, and its half-power beamwidth (HPBW) is 98.20º over a 176º 3-dB AR beamwidth.

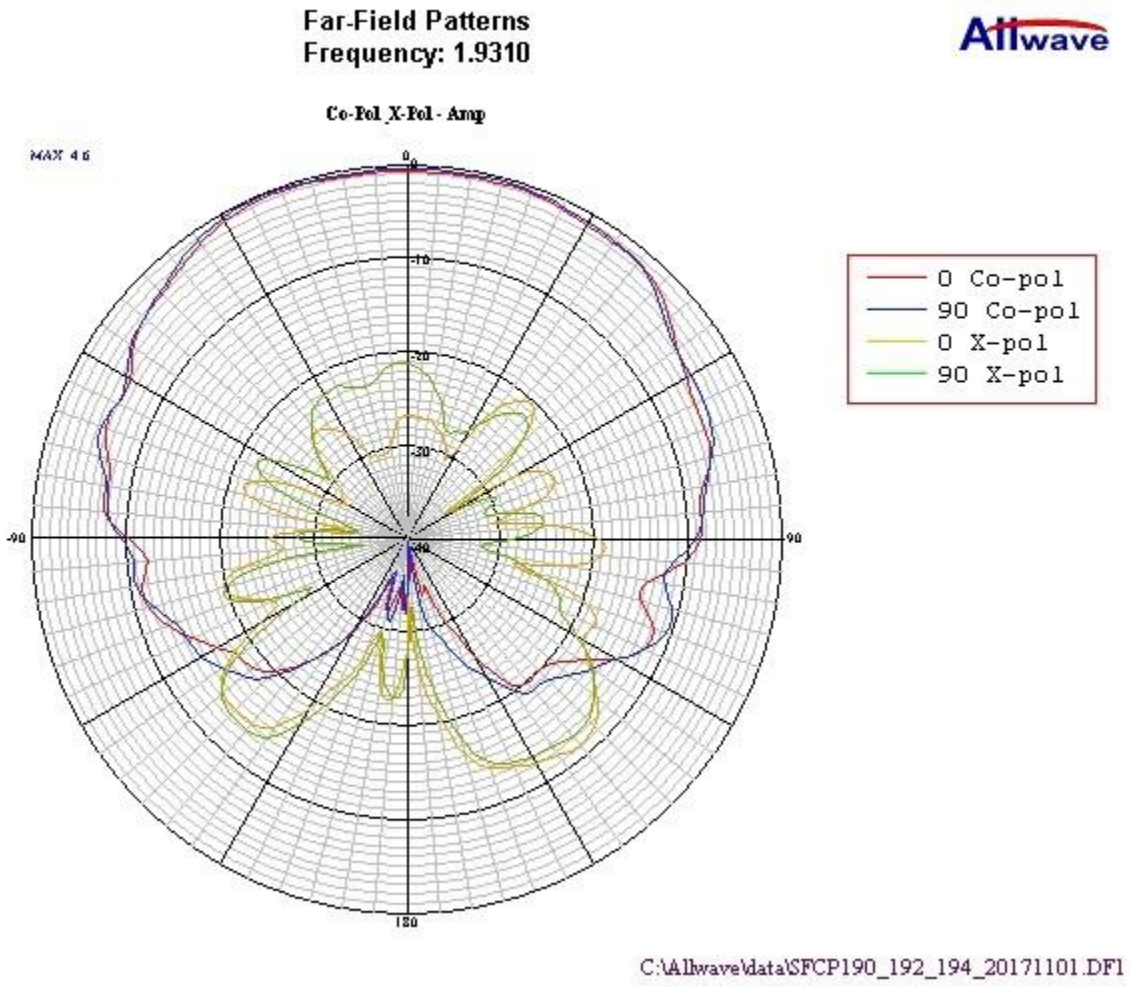

Figure 2.12 Measured radiation pattern of the antenna fabricated based on the original design. 0º and 90º are the φ angles in the spherical coordinate measurement system; the co-pol is set as RHCP and thus the X-pol is LHCP.

Figure 2.13 shows the measured and simulated AR of the proposed antenna. The minimum AR is 0.56 dB, indicating good circular polarization, with a maximum antenna gain appearing at 1.931 GHz. The 3-dB and 6-dB AR bandwidths are 13 and 29 MHz, respectively.

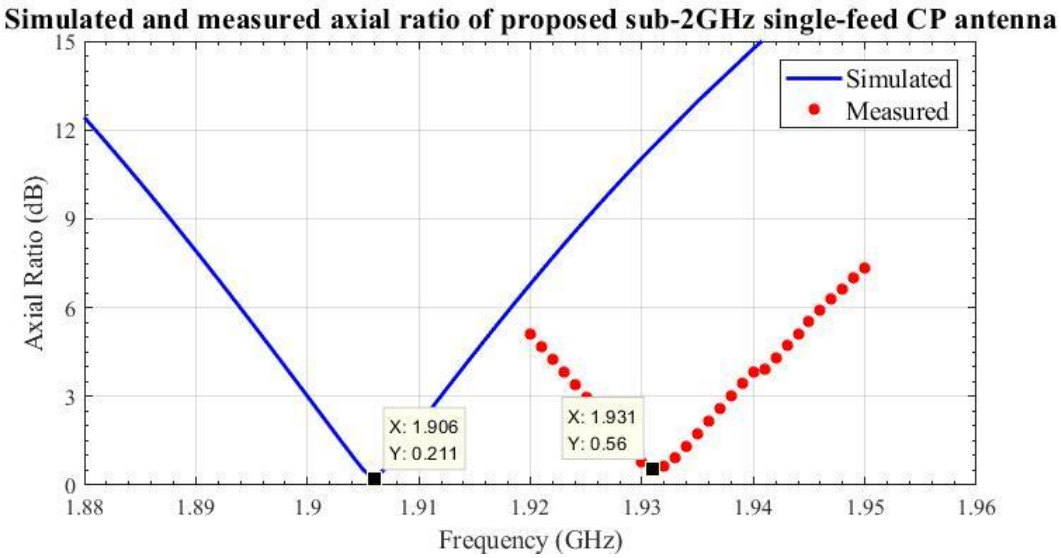

Figure 2.13 Measured AR of the antenna fabricated using the original design.

2.2.4 Summary and Conclusion

The results indicate a 1% mismatch in the center frequency between the measured and simulated results and a 0.35 dB mismatch in AR. There are several possible reasons for these mismatches. The most likely cause is imperfections in the fabricating process related to fabrication accuracy and methodology. The proposed antenna was fabricated using a milling machine; thus, during the operation, a part of the substrate would be removed by the milling head, creating an nonuniform substrate distribution close to the

patch edges. This nonuniformity could alter the fringe effect and cause a frequency shift. Additionally, the simulation assumes typical material data, though this may vary in practice.

In general, the fabricated antenna corresponds to the simulation. Some of its specifications are worse because the simulation represents an ideal case; this difference is acceptable and often happens during antenna fabrication. The antenna specifications are shown in Table 2.3.

Table 2.3 Comparison of simulated and fabricated antennas.

	Measurement	Simulation
Center frequency	1.931 GHz	1.906 GHz
Minimum AR	0.56 dB	0.21 dB
3dB/6dB AR bandwidth	13 MHz / 29 MHz	15 MHz / 31 MHz
3dB/6dB AR bandwidth in %	0.67% / 1.5%	0.78% /1.62%
RL in AR bandwidth	< -17 dB	< -20 dB
3dB Beamwidth	98.20˚	92˚
Directivity	6.21 dB	6.42 dB
Gain	5.7 dB	5.83 dB
Efficiency	88.96%	88.02%

Compared to other popular SF CP antennas with the same substrate thickness and feeding method, the proposed antenna results in a significant improvement in the AR bandwidth. The change amounts to 291.2% relative to a truncated corner square patch, and 191.4% relative to a diagonal-fed nearly square patch. In addition, the bandwidth performance is very close to the CP antenna with thicker substrate, knowing that the thicker in substrate, the higher in bandwidth, but lower in antenna efficiency.

Table 2.4 Performance comparison with other common SF CP antennas.

	This work	Diagonal-fed nearly square	Truncated corners	Diagonal slot 1/8” thickness of substrate
Center frequency	1.931 GHz	3.166 GHz	3.175 GHz	3.13 GHz
3dB / 6dB AR bandwidth in %	0.67% / 1.5%	0.35% / 0.67%	0.23% / 0.92%	0.67% / 1.2%
Minimum AR	0.15	0.25	0.15	0.2
Beamwidth	104˚	140˚	138˚	124˚

CHAPTER 3

CIRCULARLY POLARIZED MICROSTRIP STANDING-WAVE ARRAY ANTENNA

In a phased array antenna, each radiation element is excited by an input wave with a specific magnitude and phase from a microstrip line feeding network. Such a feeding network requires a number of quarter-wavelength transmission lines, which leads to high configuration complexity and extra aperture space and often produces spurious undesirable radiation, which lowers the antenna's efficiency [41-42].

3.1 Linear Polarized Standing-Wave Array Antenna

A standing wave, also known as a stationary wave, is a wave in which the peaks (or any other points on the wave) do not move spatially with time. This type of wave was first characterized by Michael Faraday in 1831. Faraday observed standing waves on the surface of a liquid in a vibrating container. The amplitude of the wave may change over time, but its phase remains constant. The locations at which the amplitude is always zero are called nodes, and the locations where the amplitude is maximized are called antinodes. Figure 3.1 depicts a standing wave.

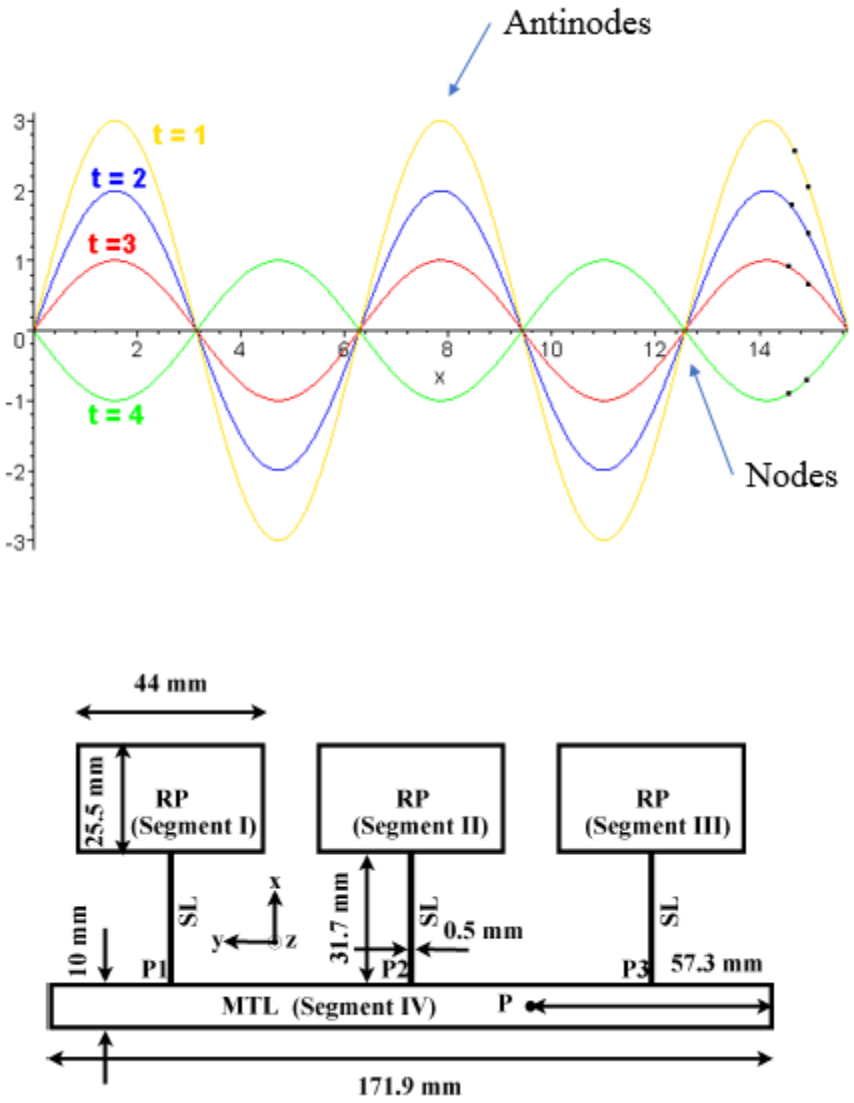

Figure 3.1 Diagram of a standing wave over time and a linear standing-wave array antenna [46].

3.1.1 Linear standing-wave array antennas

In a linear standing-wave array, the elements are fed and placed along a transmission line with half-waveguide wavelength spacing (antenna elements placed on both sides of transmission line) or one-waveguide wavelength spacing (all elements placed

on one side of the transmission line) to produce maximum radiation at the broadside [43-46].

3.1.2 Two-dimensional standing-wave array antennas

For two-dimensional standing wave arrays, the radiating elements must be arranged according to planar geometry. A feeding network in which a standing wave is formed connects the radiating patches with equal magnitudes and equal (or opposite) phases for maximum directivity. Therefore, microstrip dividers and quarter-wavelength transmission lines are not necessary in a simplified feeding network, and the resulting antenna has a relatively simple configuration and enhanced radiation efficiency [47-48].

The concept of standing-wave array antennas was developed at the SMU antenna lab [47]. In this new array structure, a high-order standing wave is excited to produce a focused beam. To verify the concept in a simple manner, a five-patch microstrip array is considered, as shown in Figure 3.2. The cavity model is used to illustrate the principle of antenna operation. In the new structure, the cavity model for a single-patch antenna is extended to a five-patch array antenna, for which the antenna cavity model would be much higher. As shown in Figure 3.2, the center patch is excited by a coaxial feed, and the surrounding elements are connected by two crisscrossing transmission lines between the four corners of the center patch. Multiple reflections occur on the connecting lines to form a standing wave within the antenna cavity, which consists of five identical square patches and four connecting transmission line networks. The data from the measured radiation patterns and input impedance degrees are generally consistent with the theoretical values, confirming the presence of a standing wave in the antenna cavity.

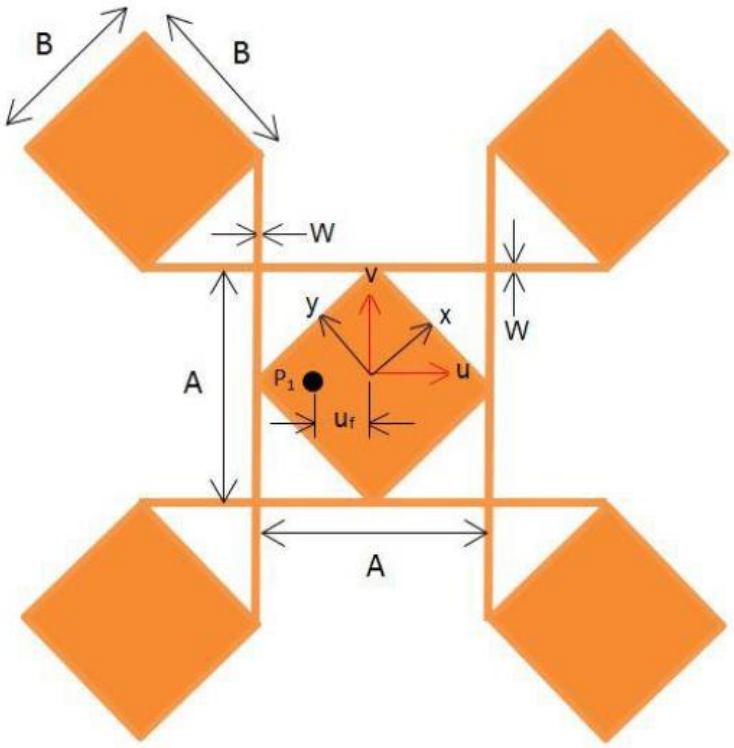

Figure 3.2 Five linearly polarized patches in a standing-wave array antenna.

3.2 Circularly Polarized Standing-Wave Array Antenna

3.2.1 Design and simulation

As explained in Section 1.3, to realize a circularly polarized (CP) antenna, the radiating electric field from an antenna should have two orthogonal components of the same magnitude and a 90° phase difference. In a conventional CP array antenna, all radiating elements must be designed to produce CP radiation. However, given the unique properties of a standing wave antenna, a CP array can be produced by replacing only one element, which is typically the one located at the array's center. Based on this scheme, the

proposed array antenna has substantial advantages relative to conventional arrays in terms of fabrication and antenna efficiency.

The five patches in the standing wave array developed in the SMU antenna lab are linearly polarized. CP radiation would result if the center patch were replaced by the previously designed SF CP microstrip antenna, yielding a simple SF CP standing wave microstrip array antenna (SF CP SWA antenna).

Because the center patch is extended by the standing wave transmission line to the surrounding parasitic patches, the feeding point needs to be refined by moving it closer to the corner. In addition, the radius of the circular slots and the distance between the two slots also must be modified to yield a good AR.

The design characteristics are shown in Table 3.1.

Table 3.1 Design parameters of sub-2GHz single feed standing-wave array CP antenna.

Items	Parameter Name	Value (mm)
Length of square patch	L	40
Radius of circle slot	Ra	3.4
Distance to patch center	CC	13
Feeding point in x-axis	Uf	8.6
Feeding point in y-axis	Vf	8.6
Width of transmission line	WTL	2

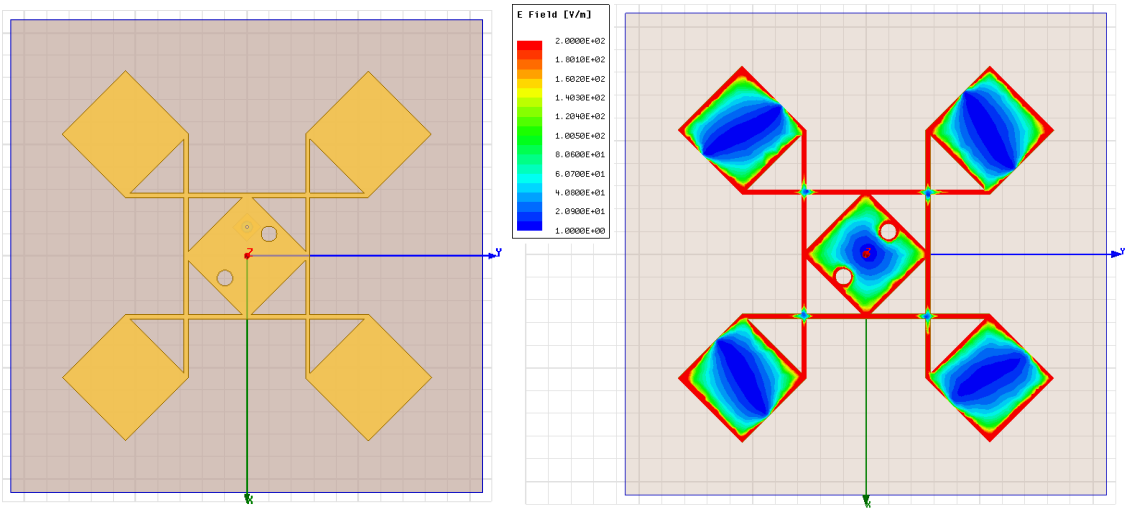

Figure 3.3 Proposed circularly polarized standing-wave array antenna and complex magnitude of the E-field of the antenna patch.

As shown in Figure 3.3, the complex magnitude E-field distribution of the center patch in the standing-wave array antenna is similar to that of the single CP microstrip antenna described in Section 2.2.2 and shown in Figure 2.7(a). Here, the center patch becomes a feed to the nearby four radiating elements connected by transmission lines, resulting in a relatively compact, high-gain CP antenna.

The complex magnitude of electric field distribution in HFSS shows that the electric field is CP in the center patch and linearly polarized in the surrounding four patches, which are grouped into two orthogonal directions, thereby forming a circular polarized wave.

Figure 3.5 shows the typical radiation pattern of an array antenna with high directivity compared to one single-patch antenna. As expected, the simulation results demonstrate an excellent AR (Figure 3.4).

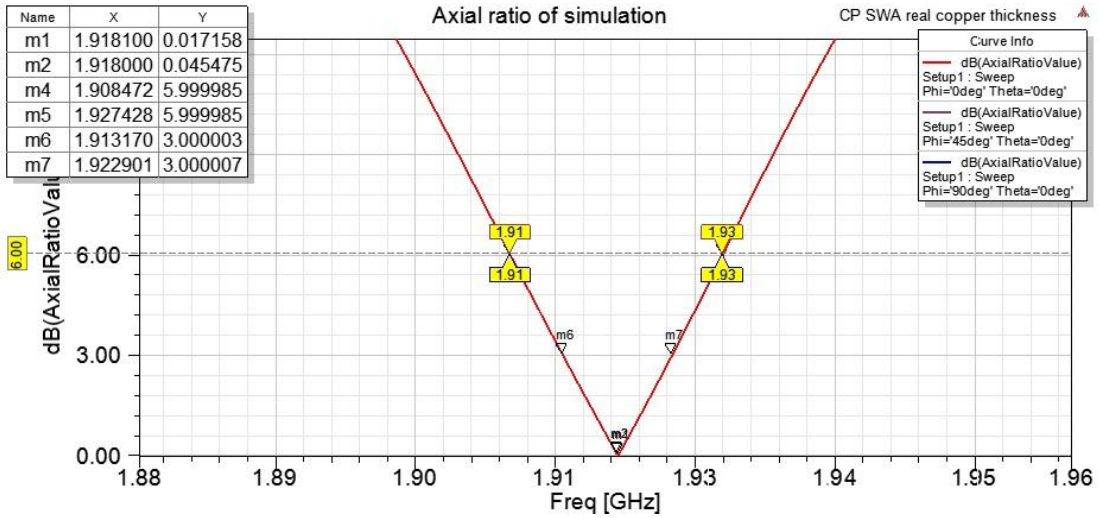

Figure 3.4 Simulation results for the AR after an optimistic analysis.

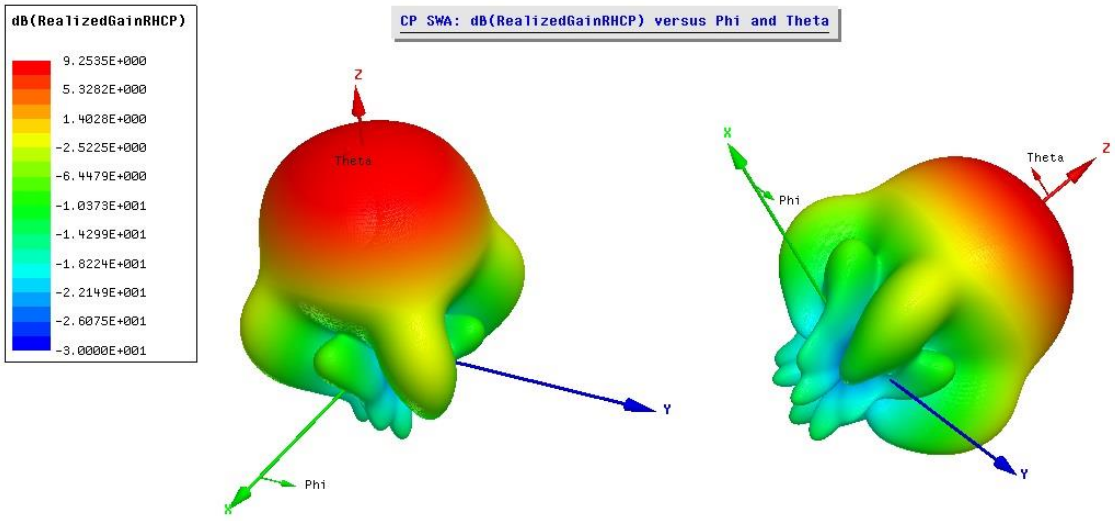

Figure 3.5 Simulated 3D realization of the RHCP gain at 1.918 GHz.

3.2.2 Measurement

The antenna was fabricated according to the parameters established during simulation. The fabricated array antenna using same substrate with single CP patch antenna introduced in chapter 2. Dimensions are followed the values shown in Table 3.1, which are the optimized results of simulation. The feed point locates on a diagonal line of the central element with 8.6 mm to the element edges. The diameter of the SMA feed pin is p = 1.27 mm. The size of the ground plane is 200 mm x 200 mm. The measured S11 and Smith charts are similar to the simulated results, shown in Figure 3.6. The two concave areas in the return loss plot indicate that two modes were excited on different resonant frequencies. The twisting trace in the Smith chart confirms this result; in general, the best AR occurs at the tip of the kink.

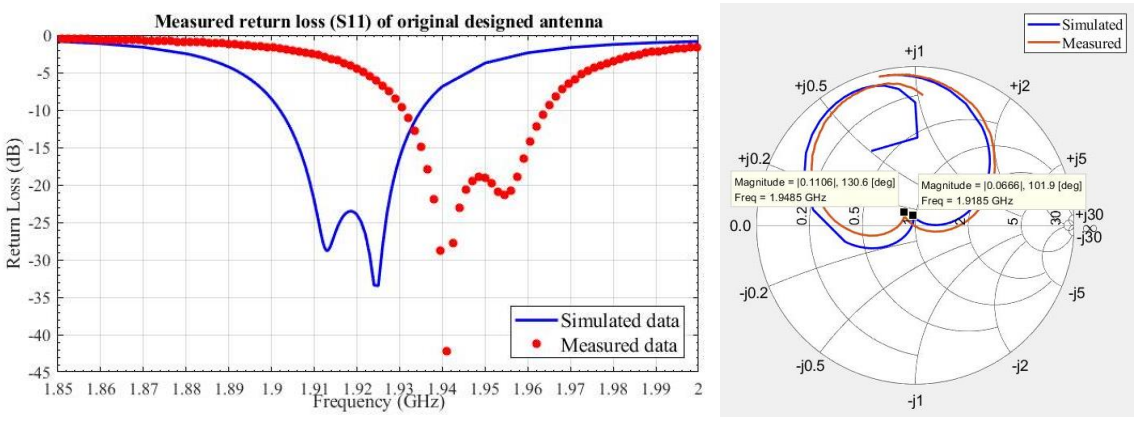

Figure 3.6 Measured and simulated S11 and Smith chart of proposed antenna.

Figures 3.7 and 3.8 show that the antenna meets the design index results, with a good AR and good gain.

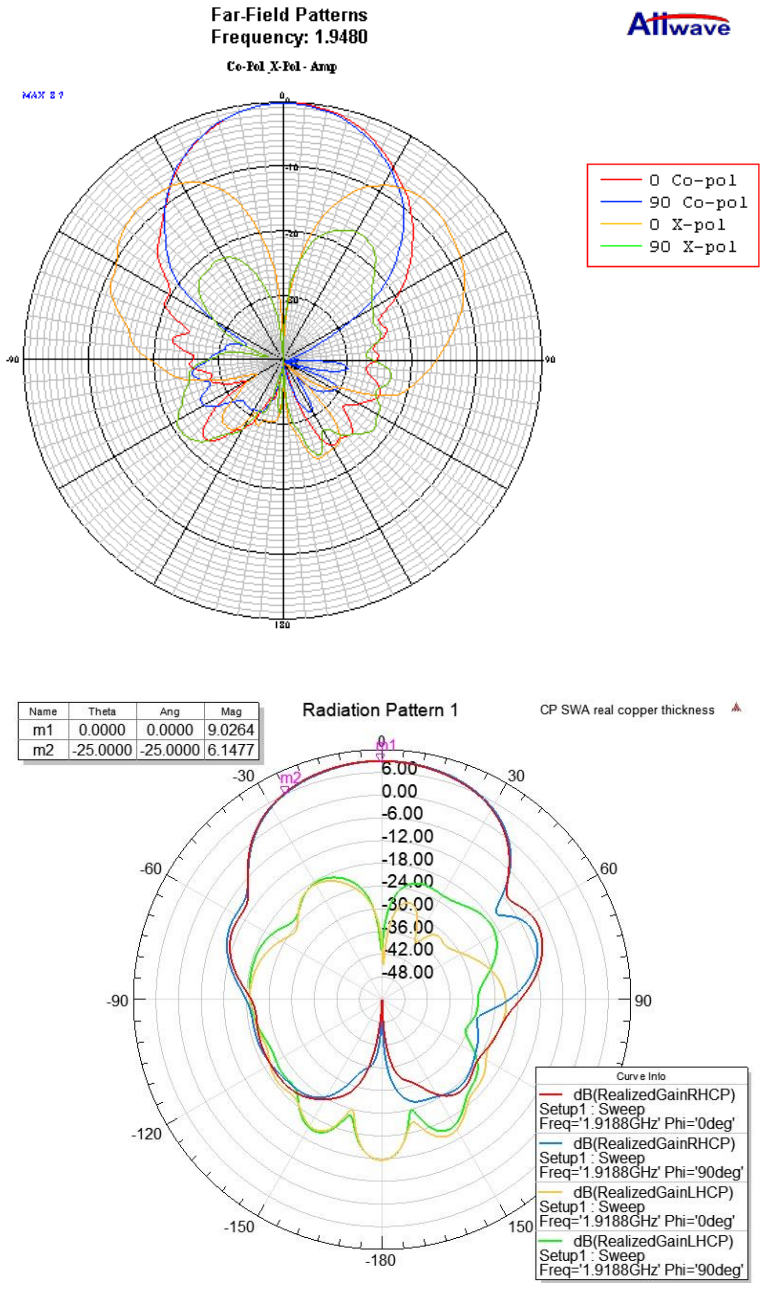

Figure 3.7 Measured and simulated radiation pattern of the proposed antenna; 0º and 90º are the φ angles in the spherical coordinate measurement system. The co-pol is set to RHCP and the X-pol is LHCP.

Figure 3.7 shows the data from the simulated and measured radiation patterns are generally consistent, confirming the presence of a standing wave in the antenna cavity. The measured minimum AR is 0.22 dB with 8.72 dB max peak gain at 1.948 GHz, yielding an 57.54% antenna efficiency, shown in Fig. 10. As contract, the simulated antenna has 0.02 dB minimum AR with 9.03 dB max RHCP gain appearing at 1.918 GHz, giving an 70.96% antenna efficiency. The measured 3-dB and 6-dB AR bandwidths are 0.47% and 0.94%, respectively.

The specifications are shown in Table 3.2.

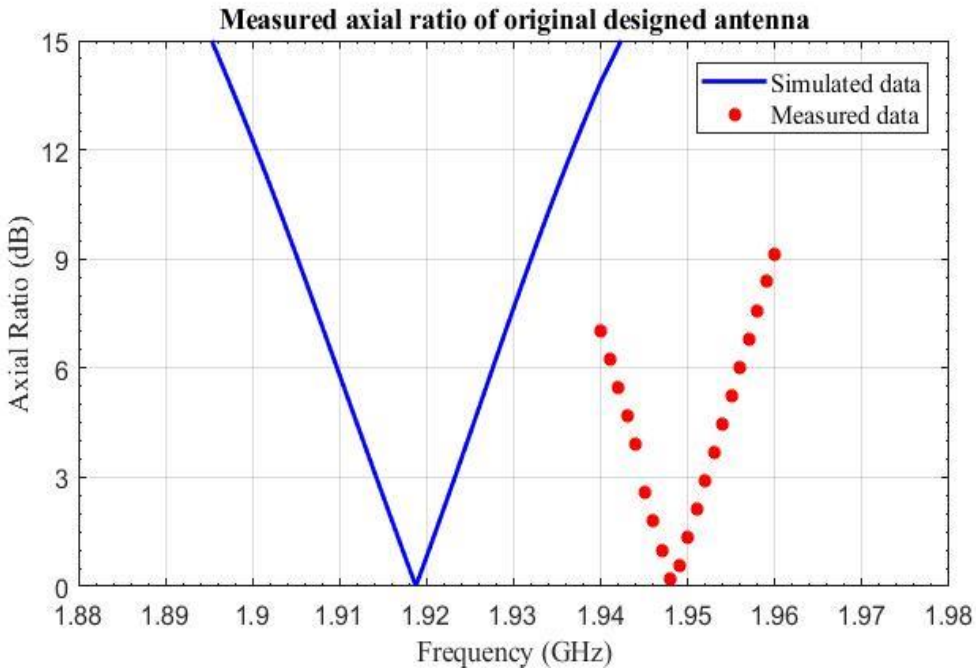

Figure 3.8 Measured and simulated AR of the proposed antenna.

3.2.3 Summary of SWA antenna

This project realizes the concept of a CP standing wave array antenna using a novel circularly polarized SF microstrip patch antenna. Because the surrounding patches work with the center patch, it is assumed that all the radiating components are in phase, providing circular polarization and maximum radiation at the boresight. Such a standing wave array antenna provides high gain and good efficiency in a relatively compact and low-profile structure compared to other CP arrays [49-51].

Table 3.2 Specifications of measured and simulated standing-wave antenna.

	Measurement	Simulation
Center frequency	1.948 GHz	1.918 GHz
Minimum AR	0.22 dB	0.02 dB
3dB/6dB AR bandwidth	8 MHz / 15 MHz	9 MHz / 18 MHz
3dB/6dB AR bandwidth in %	0.41% / 0.77%	0.47% / 0.94%
RL in AR bandwidth	< -18 dB	< -23 dB
3dB Beamwidth	42.14 °	50.4 °
Directivity	11.12 dB	10.54 dB
Gain	8.72 dB	9.13 dB
Efficiency	57.54%	70.96%

CHAPTER 4

5.8GHZ SINGLE-FEED CIRCULARLY POLARIZED MICROSTRIP PATCH ANTENNAS

In recent years, higher-frequency spectra have been opened in unlicensed bands for public usage, such as WiFi, wireless power transfer and charging, and unmanned aerial vehicles. Thus, in this section, a SF CP patch antenna working at 5.8 GHz is designed based on the same concepts described above.

4.1 5.8GHz Single-Feed CP Single Patch Antenna

4.1.1 Analysis and simulation

Chapter 2 and chapter 3 illustrate the novel structure can generate a CP wave in a SF microstrip patch antenna working below 2 GHz. Thus, the proposed 5.8 GHz CP antennas would follow the same theory and design procedure. Proper dimensions were chosen based on the calculations in Chapter 1. Following a parameter sweep in simulation, the optimum design parameters are shown in Table 4.1.

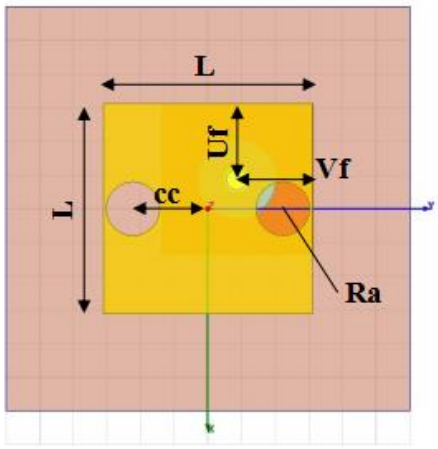

Figure 4.1 Proposed 5.8 GHz single-feed CP antenna configuration.

Table 4.1 Design parameters of 5.8GHz single-feed CP antenna.

Items	Parameter name	Value (mm)
Length of square patch	L	12.426
Radius of circle slot	Ra	1.6
Distance to patch center	CC	4.46
Feeding point in x-axis	Uf	1.74
Feeding point in y-axis	Vf	1.74

Compare to the sub-2GHz SF CP single patch antenna, the size of 5.8GHz antenna significantly decreases from 40 mm to around 12mm, following the equation (1.8). Thus, all the design parameters need to be decreased and carefully modified to achieve good axial ratio value. HFSS provides parameter sweep which is a useful function to observe the variation by changing the parameter in small linear steps.

In Figure 4.2, the S11 trace and Smith charts show a well-matched voltage standing wave ratio at 5.8 GHz. The 10-dB RL bandwidth ranges from 5.562 to 5.971 GHz, or approximately 7%.

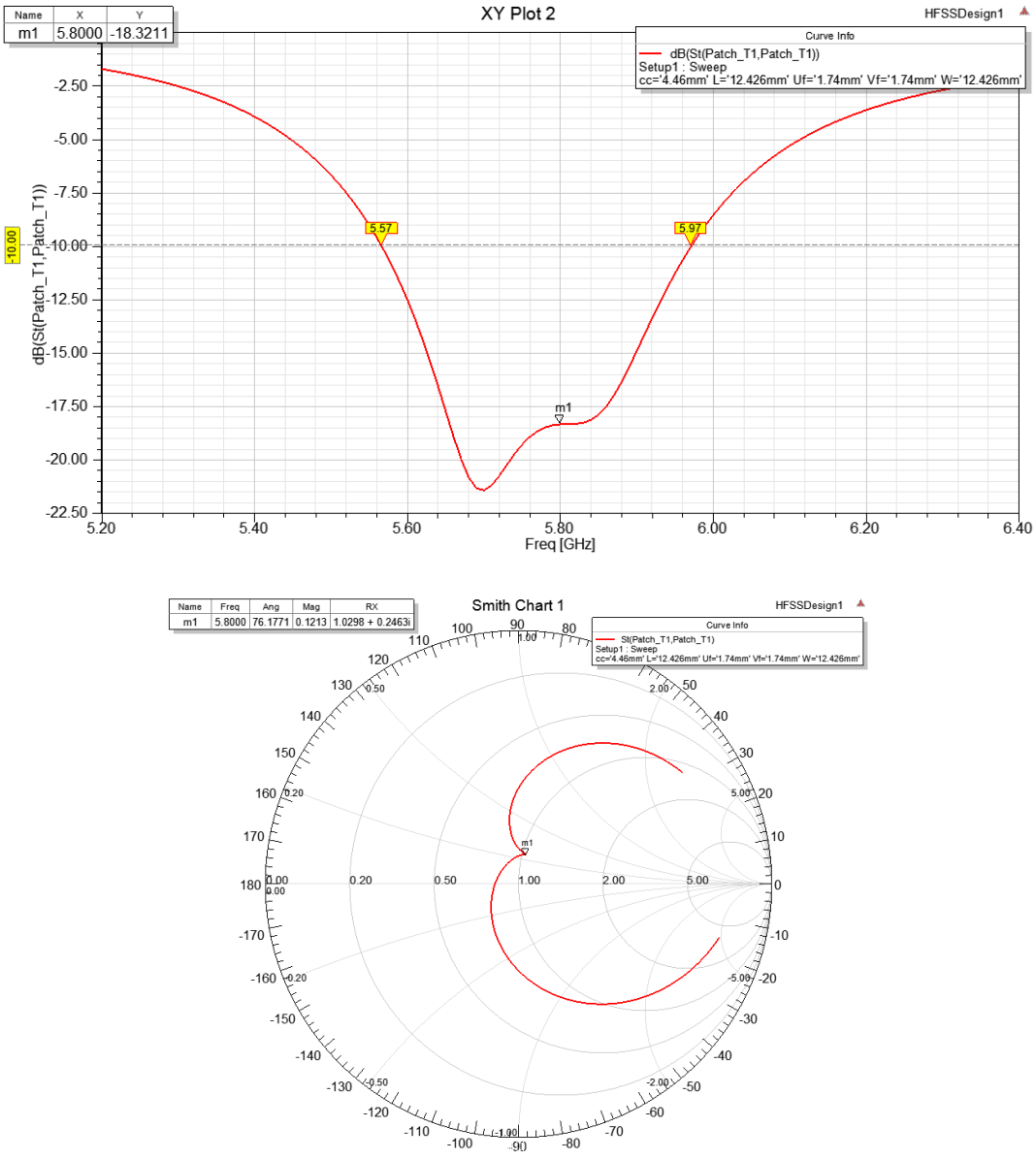

Figure 4.2 Simulated S11 RL and Smith chart of the proposed 5.8GHz SF CP antenna.

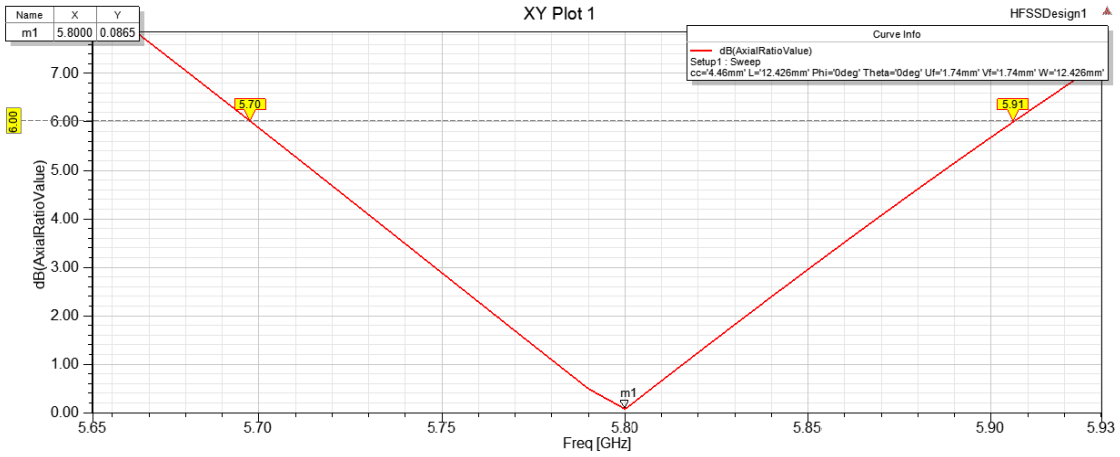

Figure 4.3 The AR of simulated result.

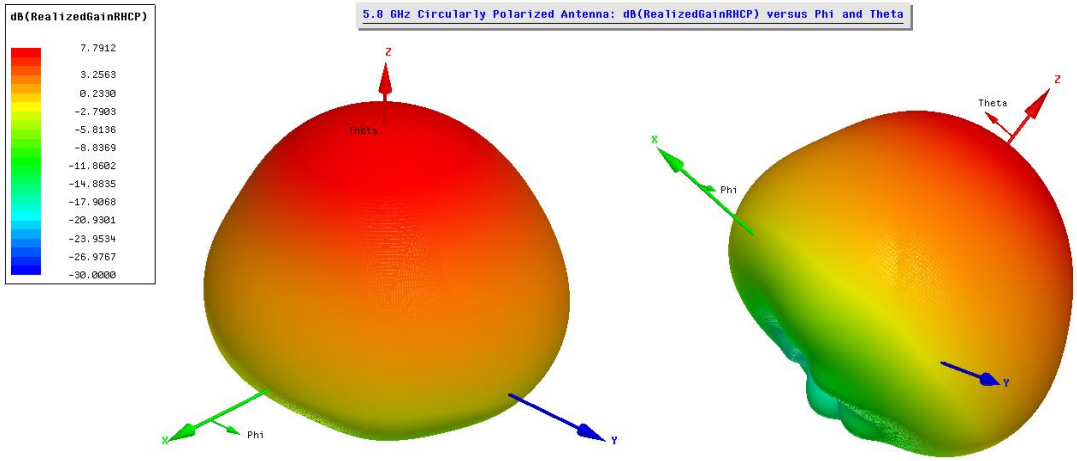

Figure 4.4 3D view of radiation pattern of the realized RHCP gain.

Figure 4.3 shows that the minimum AR is 0.04 dB at 5.8 GHz with a 3.64% 6-dB AR bandwidth. Moreover, the antenna has a mushroom-shaped radiation pattern, with 5.9 dB peak RHCP gain and 96° of half-power beamwidth, as shown in Figures 4.4 and 4.5.

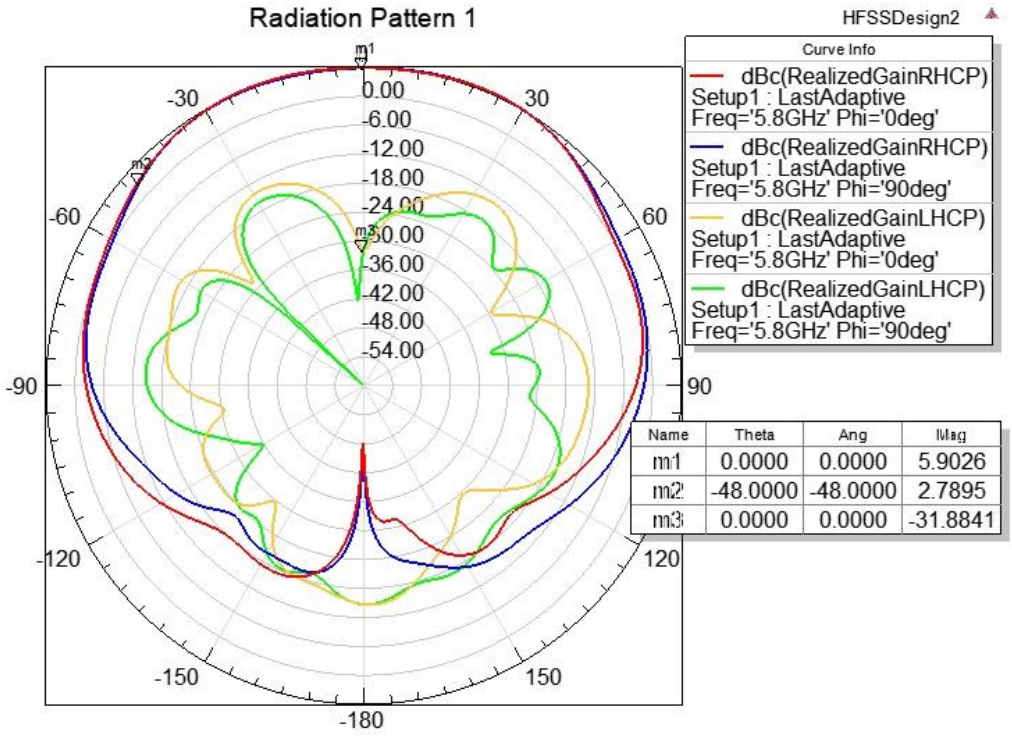

Figure 4.5 Simulated far-field radiation pattern of the realized RHCP gain.

4.1.2 Measurement

The measured S11 trace and Smith charts are shown in Figure 4.6; a 500 MHz 10-dB impedance bandwidth was observed with a return loss of -15 dB at 5.95 GHz. There is a significant kink near the desired center frequency, indicating that the two modes are working at two different resonant frequencies; this may have resulted in a proper AR. From Smith chart, the reflective coefficient indicates feed point can be modified for better impedance matching.

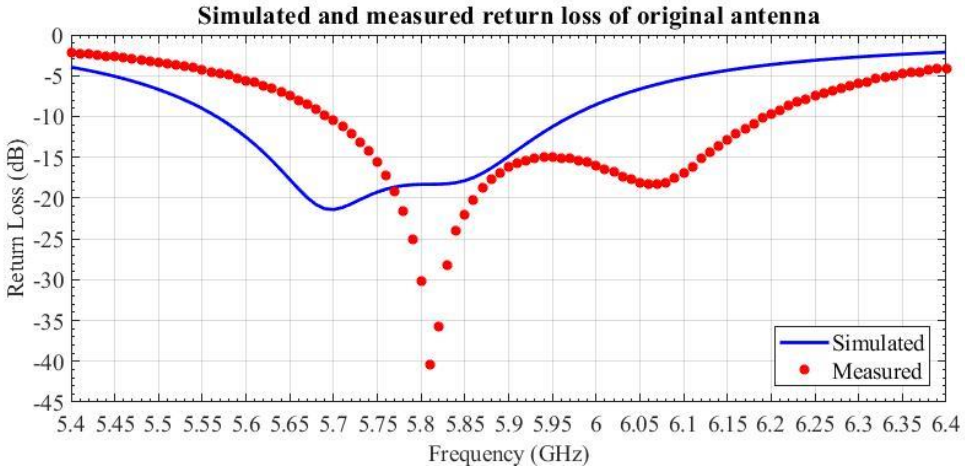

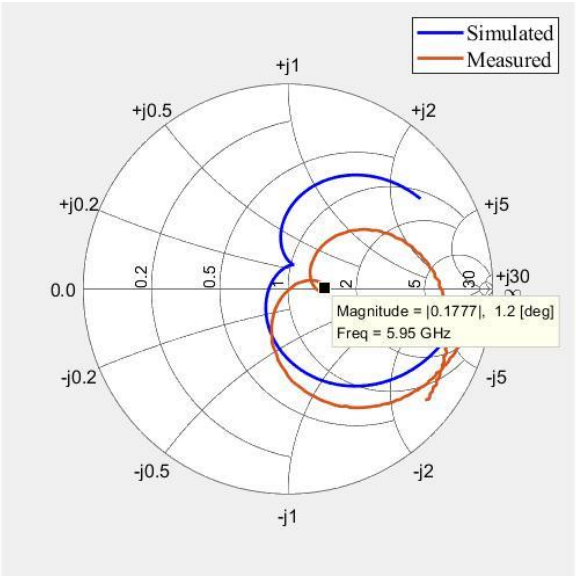

Figure 4.6 Measured and simulated S11 and Smith chart of the proposed 5.8 GHz SF CP antenna.

Figures 4.7 shows the measured radiation patterns, which has a highly consistent with simulated result, and its half-power beamwidth (HPBW) is 82.74º over a 166º 3-dB AR beamwidth. The antenna achieved a reasonable RHCP gain of approximately 5.63 dB

with a minimum AR of 0.53 dB appearing at 5.95 GHz, yielding an 69.96% antenna efficiency, shown in Figure 4.8.

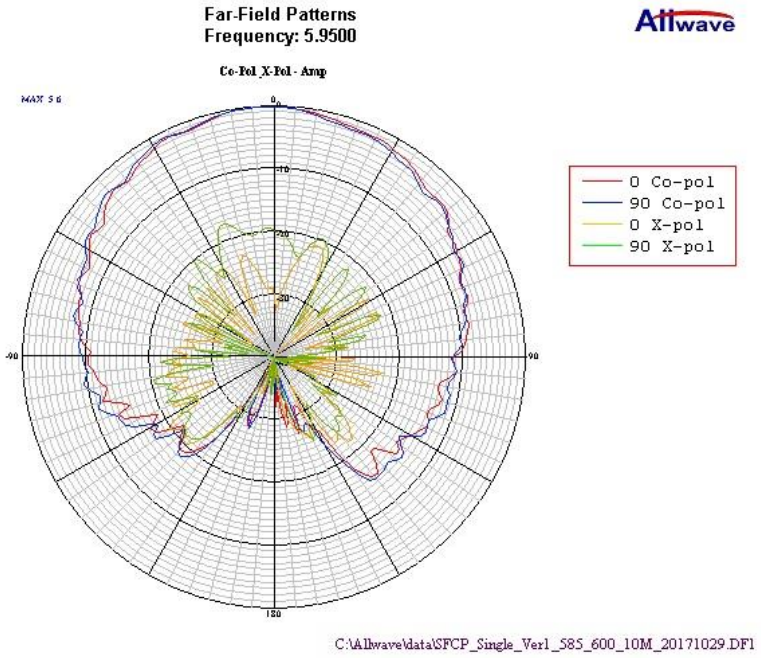

Figure 4.7 Measured radiation pattern of the proposed 5.8 GHz SF CP antenna.

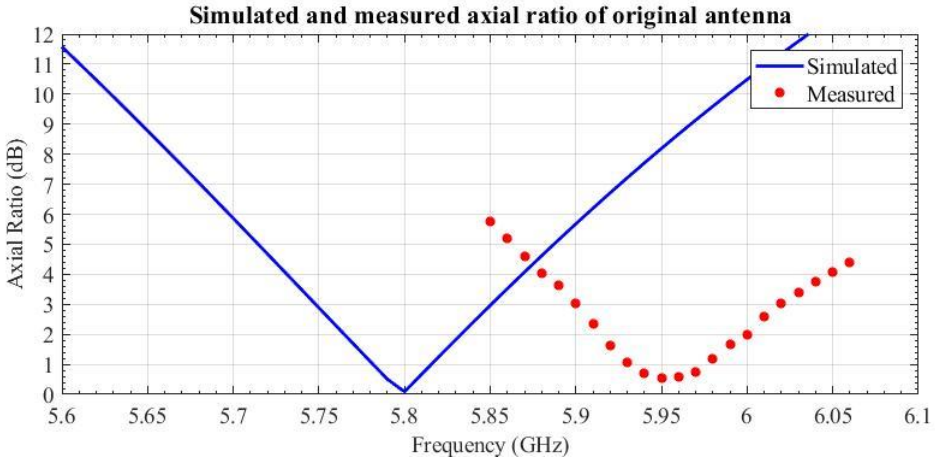

Figure 4.8 Measured and simulated AR of the proposed 5.8 GHz SF CP antenna.

4.1.3 Summary of the 5.8 GHz SF CP patch antenna

The results indicate a 1% mismatch in the center frequency between the measured and simulated results and a 0.5 dB mismatch in AR. The most likely cause is imperfections in the milling machine fabricating process related to fabrication accuracy and methodology. Additionally, the simulation assumes typical material data, though this may vary in practice.

Those differences are acceptable and often happens during antenna fabrication. In general, the fabricated antenna corresponds to the simulation.

Table 4.2 shows the summary of 5.8GHz single-feed CP patch antenna.

Table 4.2 Comparison of simulated and fabricated 5.8GHz single feed CP patch antennas.

Item	Measurement	Simulation
Center frequency	5.95 GHz	5.800 GHz
Minimum AR	0.53 dB	0.04 dB
3dB/6dB AR bandwidth	102 MHz / 208 MHz	104 MHz / 211 MHz
3dB/6dB AR bandwidth in %	1.71% / 3.5%	1.79% / 3.64%
RL in 6dB AR bandwidth	< -20 dB	< -18 dB
3dB Beamwidth	82.74˚	96˚
Directivity	7.18 dB	6.53 dB
Gain	5.63 dB	5.903 dB
Efficiency	69.96%	86.5%

4.2 5.8GHz Circularly Polarized Standing-Wave Array Antenna

4.2.1 Simulation

Implementing the above single patch at the center of an SWA antenna results in a relatively high-gain and low-profile CP antenna. The patch structure is similar to the antenna at 1.9 GHz but has smaller dimensions. CP radiation will result if the center patch is replaced by a SF CP microstrip antenna, yielding a simple SF CP standing wave microstrip array antenna (SF CP SWA antenna). Table 4.3 shows the design characteristics of this antenna.

Table 4.3 Design parameters of 5.8GHz SF CP standing-wave array microstrip antenna.

Item	Parameter name	Value (mm)
Length of square patch	L	13.12
Radius of circle slot	Ra	2.1
Distance to patch center	CC	4.18
Feeding point in x-axis	Uf	2.18
Feeding point in y-axis	Vf	2.18
Width of transmission line	WTL	1

Because the center patch is extended by the transmission lines between the standing wave and the surrounding parasitic patches, the feeding point must be refined and moved closer to the corner. The radii of the circular slots and the distance between the two slots should also be modified to yield a good AR.

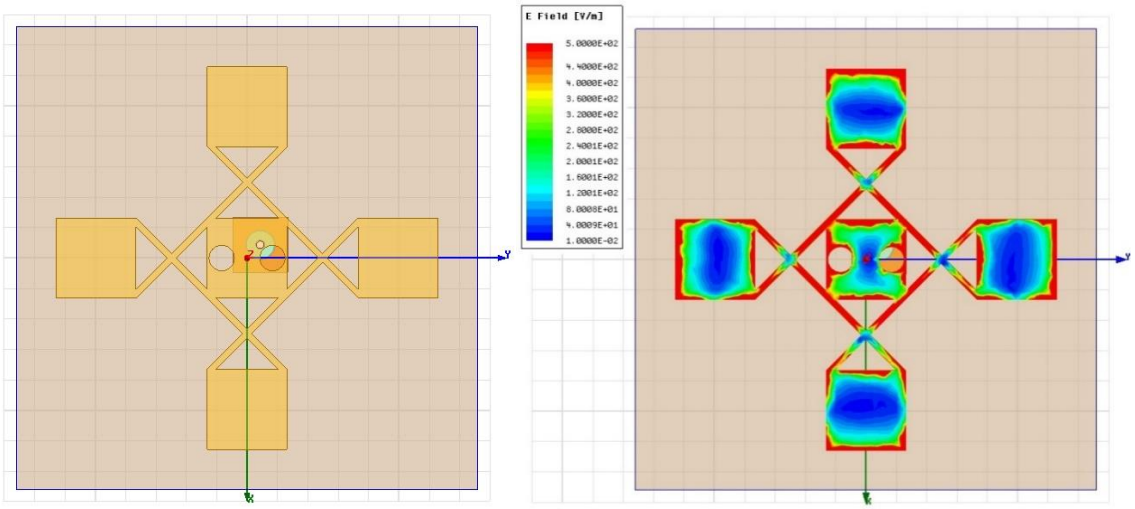

Figure 4.9 Antenna configuration and complex magnitude of E-Field distribution on patch.

The complex magnitude of the electric field distribution in Figure 4.9 shows that the electric field is CP in the center patch and linearly polarized in the surrounding four patches; these are grouped in two orthogonal directions, thus forming a circular polarized wave.

Figure 4.10 shows that the antenna has good impedance matching. Moreover, as shown in Figure 4.11, the simulation result demonstrates an excellent AR, as expected when the radius of the circle is 2.1 mm.

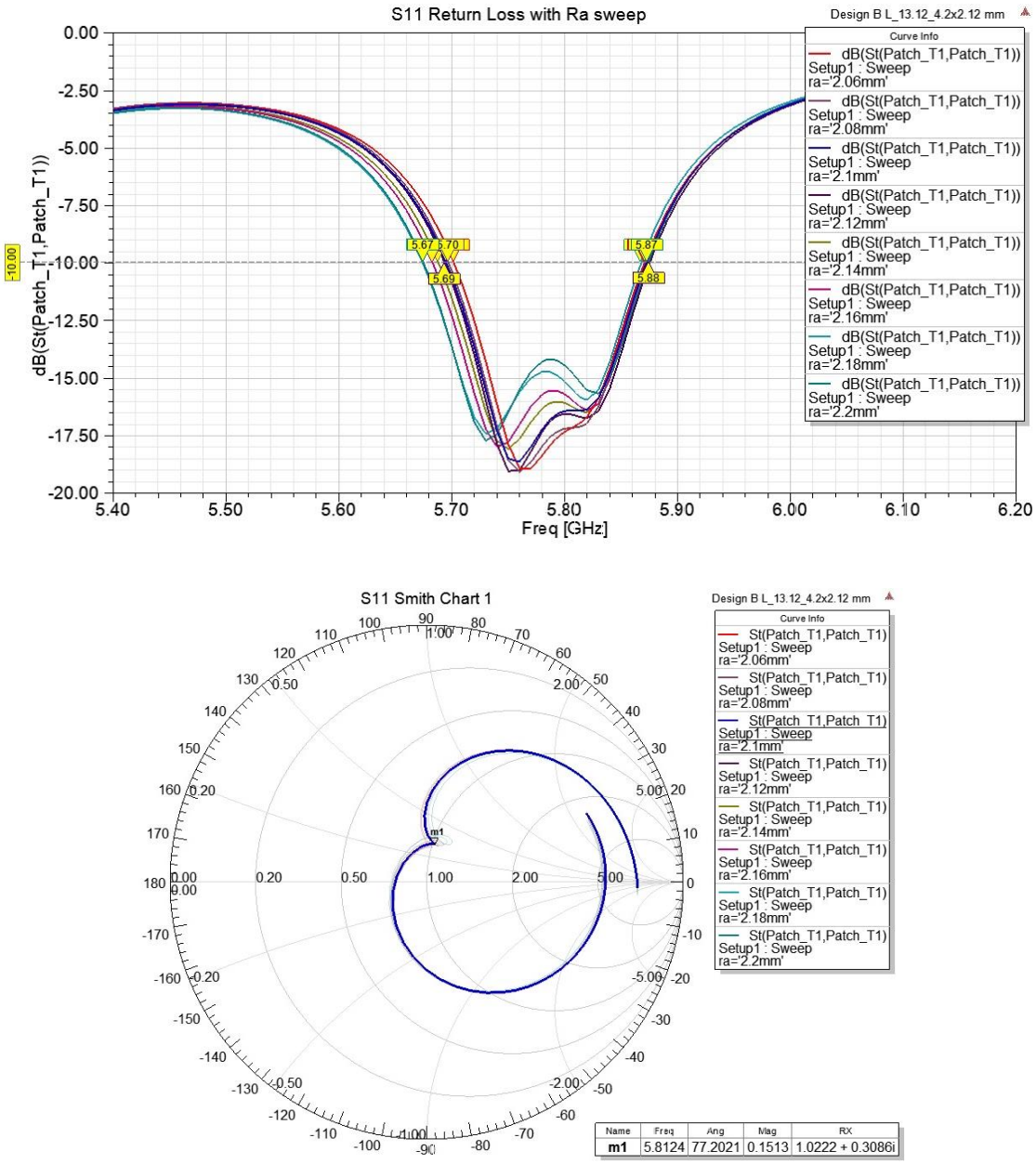

Figure 4.10 Simulated S11 return loss and Smith chart

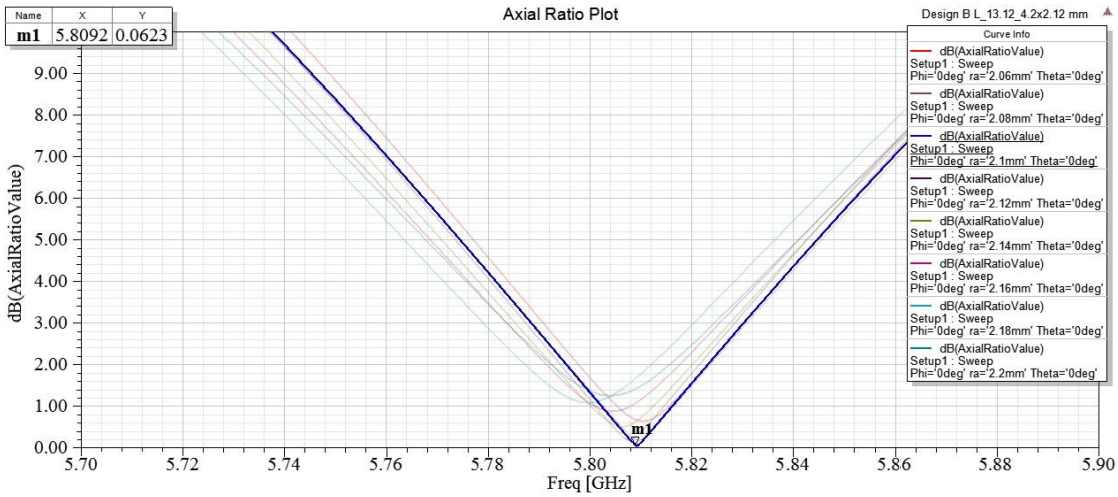

Figure 4.11 Simulated axial ratios for optimized AR

In Figure 4.12, a realized RHCP gain of up to 10.3 dB shows that the five elements work together to provide relatively high RHCP gain. The simulated radiation pattern is shown in Figure 4.13, which indicates a 46° 3-dB beamwidth with a 40-dB front-to-back ratio.

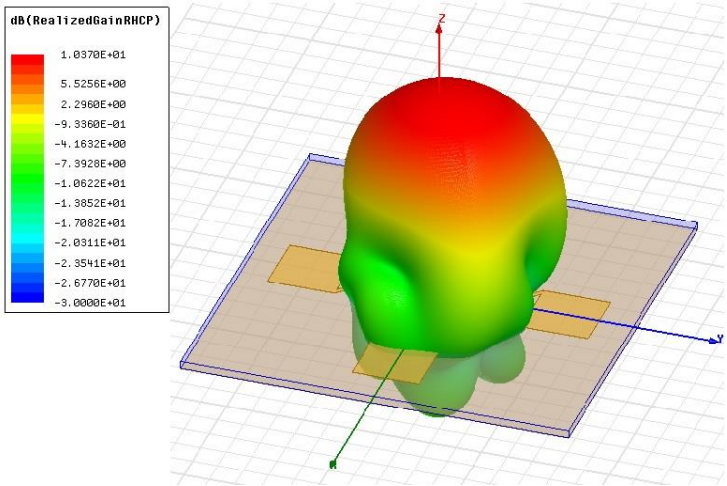

Figure 4.12 3D view of simulated radiation pattern of the realized RHCP gain.

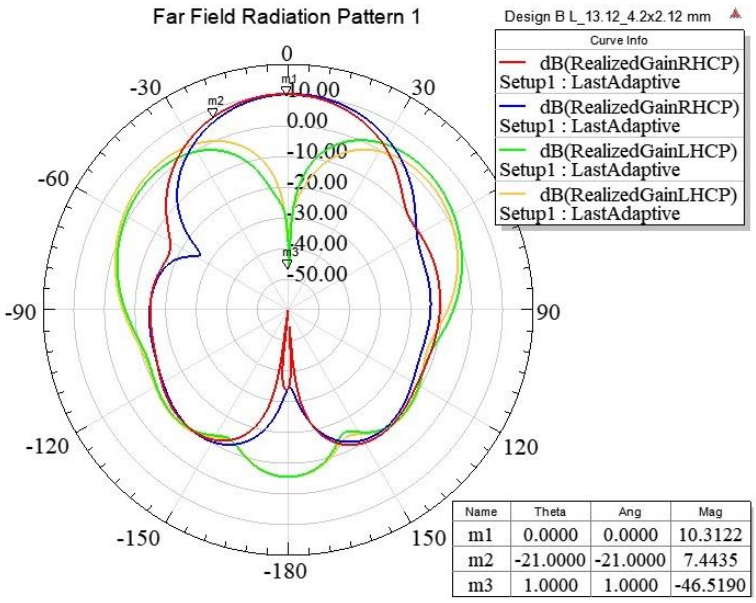

Figure 4.13 Simulated far-field radiation pattern of realized RHCP/LHCP gain.

4.2.2 Fabrication and Measurement Result

The proposed antenna, which was based on the simulation parameters, was fabricated in the Antenna Fabrication Lab at the Lyle School of Engineering, SMU, using an LPKF ProtoMat M60 milling machine. The measurement work was conducted at SMU's antenna anechoic chamber and directly tested using a far-field scan by the Allwave antenna measurement system.

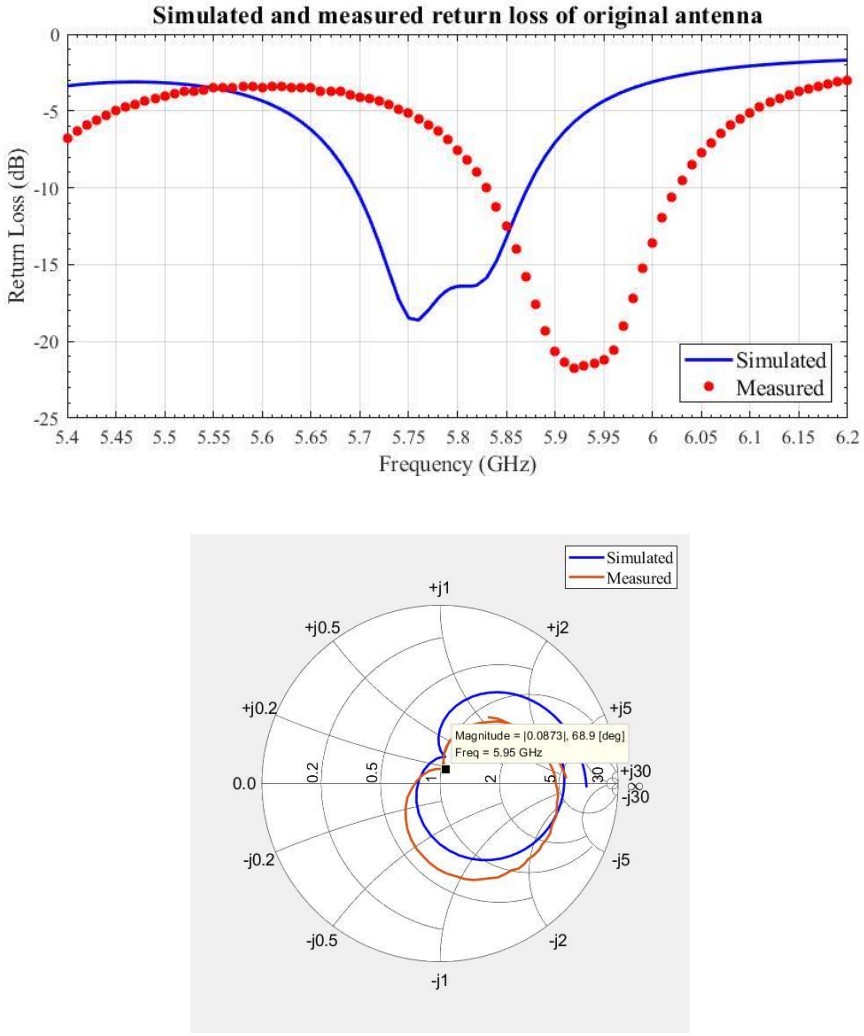

Figure 4.14 Simulated and measured S11 of the proposed 5.8GHz CP SWA antenna.

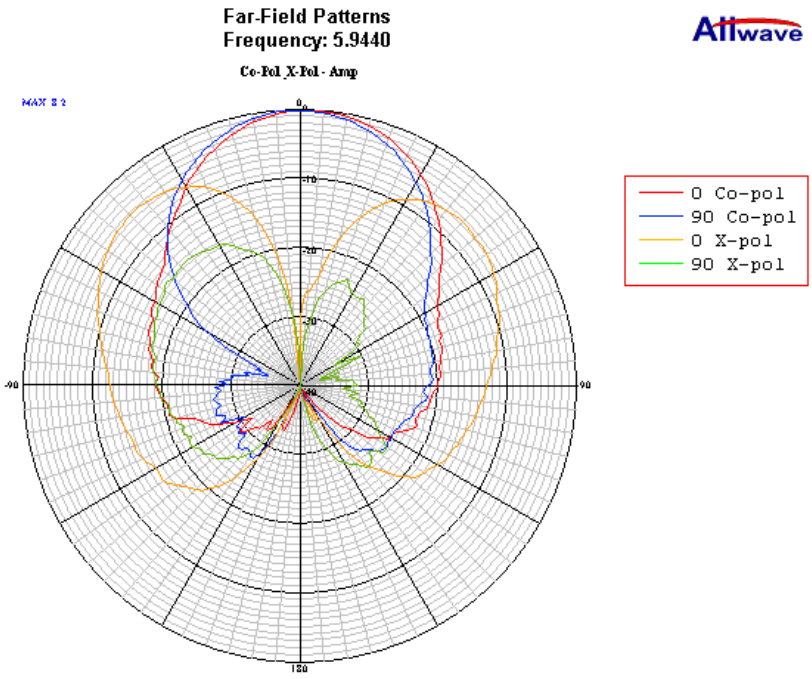

Figure 4.15 Measured radiation pattern of proposed 5.8GHz CP SWA antenna.

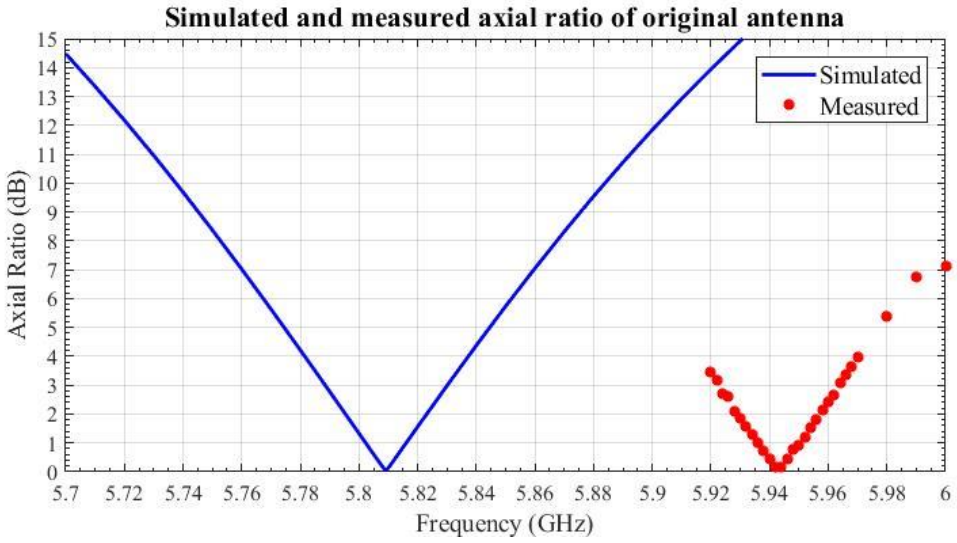

Figure 4.16 Simulated and measured AR of the proposed 5.8GHz CP SWA antenna.

The measured data shown in Figures 4.14 to 4.16 indicate that the antenna has a well-matched input feed, with S11 less than -20 dB. A perfect 0.15 dB axial ratio has been achieved at 5.942 GHz with an 8.66 dB RHCP gain. And the 6dB AR bandwidth is close to 1.4%.

4.3 Conclusion

In this project, the concept of the CP standing wave array antenna was realized using a novel circularly polarized SF microstrip patch antenna. Because the surrounding patches work with the center patch, it was assumed that all radiating components were in phase to provide circular polarization and maximum radiation at the boresight. This standing wave array antenna provides high gain and good efficiency in a relatively compact and low-profile structure compared to other CP arrays [49-51]. Table 4.4 summarizes the characteristics of the proposed 5.8 GHz SF CP SWA microstrip patch antenna.

Table 4.4 Spec comparison of the simulated and measured 5.8GHz CP SWA antenna.

Item	Measurement	Simulation
Center frequency	5.942 GHz	5.809 GHz
Minimum AR	0.15 dB	0.06 dB
3dB / 6dB AR bandwidth	40 MHz / 83 MHz	42 MHz / 86 MHz
3dB / 6dB AR bandwidth in %	0.67% / 1.4%	0.72 % / 1.48%
RL in 6dB AR bandwidth	< -20 dB	< -16 dB
3dB beamwidth	42.2˚	46˚
Directivity	10.44 dB	11.01 dB
Gain	8.66 dB	10.31 dB
Efficiency	66.47%	87.15%

CHAPTER 5

DISCUSSION

5.1 Conclusions

This dissertation presents several SF circularly polarized (CP) microstrip patch antennas based on a novel configuration—a diagonal feed through a square patch with two circular slots. A substantial increase in CP bandwidth is demonstrated. For high-gain applications with compact structures, the SF CP microstrip antenna can be applied using the standing wave array antenna developed at SMU. For this antenna, only the center element is replaced with the novel CP patch. Signals are first transmitted to the CP patch from a subminiature version A connector, after which the patch excites surrounding parasitic elements—regular square patches—through a standing wave transmission network. Thus, the combination of the center CP patch and the parasitic regular patches results in a high-gain CP antenna with a single feed in a simple and compact structure. Simulation results demonstrate the feasibility of the concept, and the measured data are generally consistent with the simulated results, validating the concept.

5.2 Future Work

Future studies will focus on replacing the excitation method and enhancing the bandwidth. Probe-fed approaches have limited bandwidth and are inconvenient for commercialization. In addition, several bandwidth-enhancement techniques exist based on a microstrip line feed, such as proximity feeding and aperture feeding. Therefore, the excitation using a probe feed should be replaced with a microstrip line feed. Due to the specific structure of the novel CP prototype, many well-developed bandwidth-enhancement techniques may not be applicable. Thus, the CP bandwidth should also be improved. Another interesting avenue for improvement is adaptive or active frequency selection, which could indirectly extend the working bandwidth of the antenna. This is common practice for linearly polarized microstrip antennas, but rare in CP antennas. At last, a 28 GHz patch with presented concept of single-feed CP antenna would be simulated and fabricated for the millimeter-wave applications.

APPENDIX

A. MATLAB CODE FOR SINGLE PATCH RECTANGULAR MICROSTRIP ANTENNA RADIATION PATTERNS

```
%*****************************************************************
%  Appendix A
%  RADIATION PATTERNS FOR SINGLE PATCH RECTANGULAR MICROSTRIP
%  ANTENNA BASED ON CAVITY MODEL
%
%     ** INPUT PARAMETERS
%     1.  FREQ   = RESONANT FREQUENCY (in GHz)
%     2.  L      = EFFECTIVE LENGTH OF THE PATCH (in mm)
%     3.  W      = WIDTH OF THE PATCH (in mm)
%*****************************************************************

clear all;
close all;
warning off;

% Input Parameters
freq=[];
while isempty(freq),
   freq=input('ENTER THE RESONANT FREQUENCY (in GHz) = ');
end;
```

```
h=[];
while isempty(h),
   h=input('ENTER THE HEIGHT OF THE SUBSTRATE (in m) = ');
end;

L=[];
while isempty(L),
   L=input('ENTER THE EFFECTIVE LENGTH OF PATCH (in mm) = ');
end;

W=[];
while isempty(W),
   W=input('ENTER THE WIDTH OF PATCH (in mm) = ');
end;

L = L.*1e-3;
W = W.*1e-3;
freq = freq.*1e9;
lambda = 3e8/freq;
ko = 2*pi/lambda;
% Eth radiating & non-radiating slots
phi1=0; phir1=phi1.*pi./180;
th1=0:360; thr1=th1.*pi/180;

X = ko.*W.*sin(thr1).*sin(phir1)/2;
Y = ko.*L.*sin(thr1).*cos(phir1)/2;
```

```
Z = i.*ko.*h./pi;
A = sqrt(2*W/L);
B = sqrt(2*L/W);

Fx1 = B.*sin(X).*Y.*cos(Y)./((pi/2).^2-(Y).^2);
Fy1 = A.*cos(Y).*sinc(X);

Eth = Z.*((Fx1.*sin(phir1))-(Fy1.*cos(phir1)));
Eth1 = abs(Eth);
Ethnorm = Eth1./max(Eth1);
EthdBtotal =20.*log10(Ethnorm);
EthdBtotal(thr1>pi/2&thr1<3*pi/2)=-60;
EthdBtotal(EthdBtotal<=-60)=-60;

% Ephi radiated & non-radiating slots

phi2=90; phir2=phi2.*pi./180;
th2=0:360; thr2=th2.*pi/180.0;

X2 = ko.*W.*sin(thr2).*sin(phir2)/2;
Y2 = ko.*L.*sin(thr2).*cos(phir2)/2;
Fx2 = B.*sin(X2).*Y2.*cos(Y2)./((pi/2).^2-(Y2).^2);
Fy2 = A.*cos(Y2).*sinc(X2./pi);

Eph                                                                    =
Z.*((Fx2.*cos(phir2).*cos(thr2))+(Fy2.*sin(phir2).*cos(thr2)));
Eph1 = abs(Eph);
Ephnorm = Eph1./max(Eph1);
EphdB = 20.*log10(Ephnorm);
EphdB(thr1>pi/2&thr1<3*pi/2)=-60;
EphdB(EphdB<=-60)=-60;
```

```
%%%%%%%%%%%%%%%%%%%%%%%%%%%%%%%%%%%%%%
% Co-pol & X-pol @ phi = 45 deg
%%%%%%%%%%%%%%%%%%%%%%%%%%%%%%%%%%%%%%

phi3=45; phir3=phi3.*pi./180;
th3=0:360; thr3=th3.*pi./180;

X3 = ko.*W.*sin(thr3).*sin(phir3)/2;
Y3 = ko.*L.*sin(thr3).*cos(phir3)/2;

Fx3 = B.*sin(X3).*Y3.*cos(Y3)./((pi/2).^2-(Y3).^2);
Fy3 = A.*cos(Y3).*sinc(X3);

Eth45 = Z.*((Fx3.*sin(phir3))-(Fy3.*cos(phir3)));

EthCo45 = abs(Eth45);
EthCo45norm = EthCo45./max(Eth1);
EthdB45 =20.*log10(EthCo45norm);
EthdB45(thr1>pi/2&thr1<3*pi/2)=-60;
EthdB45(EthdB45<=-60)=-60;

phi4=45; phir4=phi4.*pi./180;

X4 = ko.*W.*sin(thr3).*sin(phir4)/2;
Y4 = ko.*L.*sin(thr3).*cos(phir4)/2;

Fx4 = B.*sin(X4).*Y4.*cos(Y4)./((pi/2).^2-(Y4).^2);
Fy4 = A.*cos(Y4).*sinc(X4);
```

```
      Eph45=Z.*((Fx4.*cos(phir4).*cos(thr3))+(Fy4.*sin(phir4).*cos(thr3
)));
      Eph45 = abs(Eph45);
      Eph45Xpol = Eph45./max(Eth1);
      EphdB45 = 20.*log10(Eph45Xpol);
      EphdB45(thr1>pi/2&thr1<3*pi/2)=-80;
      EphdB45(EphdB45<=-60)=-60;

      %%%%%%%%%%%%%%%%%%%%%%%%%%%%%%%%%%%%%%%%%%%%%%%%%%%%%%%%
      % Radiation Plots
      %%%%%%%%%%%%%%%%%%%%%%%%%%%%%%%%%%%%%%%%%%%%%%%%%%%%%%%%
      figure
      polar_db(th1,EthdBtotal,-60,0,4,'-')

      figure
      polar_db(th2,EphdB,-60,0,4,'-')

      figure
      polar_db(th3,EthdB45,-30,0,4,'-')

      figure
      polar_db(th3,EphdB45,-30,0,4,'-')
```

B. MATLAB CODE FOR CALCULATING QUALITY FACTOR (Q) FOR SINGLE PATCH RECTANGULAR MICROSTRIP ANTENNA

```
%*****************************************************************
%  Appendix B
%  QUALITY FACTOR FOR SINGLE PATCH RECTANGULAR MICROSTRIP ANTENNA
%  BASED ON CAVITY MODEL
%
%*****************************************************************


% Input Parameters
eta = 377;
eo = 8.854e-12;
u = 4.*pi*1e-7;
s = 5.8e7;
freq = 4.75e9;
ko = 2*pi*freq/3e8;
t = 0.001575;
erff = 3.38;
L = 17.15e-3;
W = 21.25e-3;
% Integration [|Etheta|^2+|Ephi|^2]*sin(theta)
fun=@(phir,thr)((abs((ko.*t./pi).*((sqrt(2.*L/W).*(ko.*L./2).*sin
(thr).*cos(phir).*cos((ko.*L./2).*sin(thr).*cos(phir)).*sin((ko.*W./2).
*sin(thr).*sin(phir)).*sin(phir)./((pi/2).^2-
((ko.*L./2).*sin(thr).*cos(phir)).^2))-
(sqrt(2.*W/L).*sin((ko.*W./2).*sin(thr).*sin(phir)).*cos((ko.*L./2).*si
n(thr).*cos(phir)).*cos(phir)./((ko.*W./2).*sin(thr).*sin(phir))))).^2+
(abs(ko.*t./pi).*((sqrt(2.*L/W).*(ko.*L./2).*sin(thr).*cos(phir).*cos((
ko.*L./2).*sin(thr).*cos(phir)).*sin((ko.*W./2).*sin(thr).*sin(phir)).*
cos(phir).*cos(thr)./((pi/2).^2-
((ko.*L./2).*sin(thr).*cos(phir)).^2))+(sqrt(2.*W./L).*sin((ko.*W./2).*
```

```
sin(thr).*sin(phir)).*cos((ko.*L./2).*sin(thr).*cos(phir)).*sin(phir).*
cos(thr)./((ko.*W./2).*sin(thr).*sin(phir))))).^2).*sin(thr));

      Int = integral2(fun,0,2*pi,0,pi/2)

      We = 0.5.*eo.*erff.*t

      % Radiation power and Qrad Calculation

      Pr = Int./(2*eta)

      Qrad = (2.*pi.*freq.*We)./(Pr)

      % Total Quality Factor Calculation

      Qc = t.*sqrt(pi.*freq.*u.*s);

      Qd = 1./0.0021;

      Qt = ((1./Qrad)+(1./Qc)+(1./Qd)).^-1
```

C. MATLAB CODE FOR CALCULATING INPUT IMPEDANCE FOR SINGLE PATCH RECTANGULAR MICROSTRIP ANTENNA

```
%*************************************************************
%  Appendix C
%  INPUT IMPEDANCE USING CAVITY MODEL
%*************************************************************



f = 4:0.005:5;
freq = f.*1e9;
lamda = 3e8./freq;
Q = 28.82;
Q_eff = 28.49;
xo = 2.925e-3;
xo_eff = 2.925e-3;
er = 3.38;
ereff = 3.055;
h = 0.0015748;
L = 17.15e-3;
W = 21.25e-3;
Leff = 18.64e-3;
eta = 377.*(1/er)^0.5;
eta_eff = 377.*(1/ereff).^0.5;
k1 = (2.*pi.*freq.*(er).^0.5)./3e8;
k2 = (2.*pi.*freq.*(ereff).^0.5)./3e8;


ko = 2*pi./lamda;
x = complex(1,-1/Q);
x_eff = complex(1,-1/Q_eff);
```

```
k = ko.^2.*er.*x;
k_reff = ko.^2.*ereff.*x_eff;
a = 2.*pi.*freq.*4.*pi.*1e-7.*h;
ja = complex(0,-a);
b = 2./(L.*W);
c = 2./(Leff.*W);

% Term (1,0) calculation

kn = k - (pi./L).^2;
kneff = k_reff - (pi./Leff).^2;
U01 = b.*(sin((pi.*xo)./L)).^2;
U01_eff = c.*(sin((pi.*xo_eff)./Leff)).^2;
T3 = U01./kn;
T3_reff = U01_eff./kneff;
```

```
% Xf calculation

Xf = ((-eta.*k1.*h)./(2.*pi)).*(log(k1.*0.00127./4)+0.577);
Xf_eff=((-eta_eff.*k2.*h)./(2.*pi)).*(log(k2.*0.00127./4)+0.577);
jXf = complex(0,Xf);
jXf_eff = complex(0,Xf_eff);

% Zin calculation

Z = (ja.*T3);
Z_eff = (ja.*T3_reff);

Zinput = Z+jXf;
Zinput_eff = Z_eff+jXf_eff;

S11 = (Zinput - 50)./(Zinput + 50);
S11_eff = (Zinput_eff - 50)./(Zinput_eff + 50);
S11_amp = abs(S11);
S11_dB = 20.*log10(S11_amp);
S11_amp_eff = abs(S11_eff);
S11_dB_eff = 20.*log10(S11_amp_eff);

figure
plot(f,S11_dB);

figure
plot(f,S11_dB_eff);
```

REFERENCE

[1] William H. Hayt, Jr. John A. Buck, "Engineering Electromagnetics 8th Edition", International Edition 2012, McGraw-Hill Education, Chapter 11.

[2] Warren L. Stutzman, Gary A. Thiele, "Antenna Theory and Design 3rd Edition", John Wiley & Sons, Inc. Chapter 2.

[3] Simon Ramo, John R. Whinnery, Theodore Van Duzer, "Fields and Waves in Communication Electronics 3rd Edition", John Wiley & Sons, Inc. Chapter 6.

[4] John L. Volakis, "Antenna Engineering Handbook 4th Edition", McGraw-Hill, 2007

[5] Lee, Kai Fong, Luk, Kwai Man (2011), "Microstrip Patch Antennas", World Scientific, Chapter 1, pp. 8–12. ISBN 184816453X

[6] Warren L. Stutzman, Gary A. Thiele, "Antenna Theory and Design 3rd Edition", John Wiley & Sons, Inc. Chapter 11, pp465-475.

[7] D.M. Pozar, "Microstrip Antennas", Proceedings of the IEEE, Volume: 80, Issue: 1, Jan 1992, pp. 79-91.

[8] J.R. James, Peter S. Hall, Colin Wood, "Microstrip Antenna: Theory and Design", Peter Peregrinus Ltd, London, UK, 1981.

[9] Ramesh Garg, P. Bhatia, I. Bhal, A. Ittipiboon, "Microstrip Antenna Design Handbook", Artech House, 2001.

[10] D.M. Pozar, "Microwave Engineering 4th Edition", John Wiley & Sons, Inc. 2012, Chapter 5, pp. 246-250.

[11] K.M. Luk, X. Guo, K.F. Lee, Y.L. Chow, "Analysis and Design of L-Probe Proximity Fed Patch Antennas", Antennas and Propagation Society International Symposium, IEEE, July 2000.

[12] A. Hoorfar, G. Girard, A. Perrotta, "Dual Frequency Circularly Polarized proximity-fed microstrip antenna", Electronics Letters, Volume: 35, Issue: 10, pp. 759-761, 13 May 1999.

[13] D.M. Pozar, B. Kaufman, "Increasing the bandwidth of a microstrip antenna by proximity coupling", Electronics Letters, Volume: 23, Issue: 8, pp. 368-369, April 1987.

[14] D.M. Pozar, “Five novel feeding techniques for microstrip antennas”, Antennas and Propagation Society International Symposium, IEEE, Jun 1987.

[15] A. Ittipiboon, R. Oostlander, Y.M.M. Antar, M. Cuhaci, “Theory and measurement for aperture coupled microstrip antenna”, Antenna Technology and Applied Electromagnetics, IEEE Symposium, Aug 1990.

[16] Lo, Y.T., Solomon D. and Richards, W.F. "Theory and Experiment on Microstrip Antennas," IEEE Transactions on Antennas and Propagation, pp. 137-149, AP-27, 1979.

[17] A.A. Mohammad, H. Subhi, A.K. Ahmad, S.M. Juma, “Cavity model analysis of rectangular microstrip antenna operating in TM03mode”, Information and Communication Technologies, IEEE, April 2006.

[18] Hong Li Peng, Zheng Tang, Yao Ping Zhang, Jun Fa Mao, “Cavity Model Analysis of a Dual-Probe-Feed Circular Microstrip Patch Antenna”, IEEE Antennas and Wireless Propagation Letters, Vol: 15, pp. 44-47, April 2015

[19] Keith R. Carver, James W. Mink, “Microstrip Antenna Technology”, IEEE Tranz. Antennas Propag, AP-29, 1981.

[20] J. Wong, H. King, “Empirical Helix Antenna Design”, Antennas and Propagation Society International Symposium, IEEE, May 1982.

[21] R.M. Barts, W.L. Stutzman, “A Reduced Size Helical Antenna”, Antennas and Propagation Society International Symposium, IEEE, Jul 1997.

[22] P.S. Hall.: “Review of Techniques for Dual and Circularly Polarized Microstrip Antennas”, The University of Birmingham, UK

[23] HUANG, J.: ‘Circularly Polarized Conical Patterns from Circular Microstrip Antenna’, IEEE Trans. Antennas Propag, AP-32, pp. 991-994, 1984.

[24] Kin-Lu Wong, Tzung-Wern Chiou, “Broad-band Single-patch Circularly Polarized Microstrip Antenna with Dual Capacitively Coupled Feeds”, IEEE Transactions on Antennas and Propagation, Volume: 49, Issue: 1, Jan 2001.

[25] RICHARDS, W.F., LO, Y.T., and HARRISON, D.D.: ‘An Improved Theory for Microstrip Antennas and Applications’, IEEE Trans. Antennas Propag., AP-29, pp. 38-46, 1981,

[26] P. Sharma, K. Gupta, “Analysis and Optimized Design of Single Feed Circularly Polarized Microstrip Antennas”, IEEE Transactions on Antennas and Propagation, Volume: 31, Issue: 6, pp. 949-955, Nov 1983

[27] Y. T. Lo, B. Engst, R. Q. Lee, "Simple Design Formulas for Circularly Polarized Microstrip Antennas," IEE Proceedings, vol. 135, pp. 213-215, Jun. 1998.

[28] W. L. Langston, D. R. Jackson, "Impedance, Axial-ratio, and Received-power Bandwidths of Microstrip Antennas," IEEE Trans. Antennas Propag., vol. 25, pp. 2769-2773, Oct. 2004.

[29] Young-Ho Suh, Chunlei Wang, Kai Chang, "Circularly Polarized Truncated-Corner Square Patch Microstrip Rectenna for Wireless Power Transmission", Electronics Letters, Volume: 36, Issue: 7, pp. 600-602, Mar 2000.

[30] Wen-Shyang Chen, Chun-Kun Wu, Kin-Lu Wong, "Novel Compact Circularly Polarized Square Microstrip Antenna", IEEE Transactions on Antennas and Propagation, Volume: 49, Issue: 3, pp. 340-342, Mar 2001.

[31] H. Mosallaei, K. Sarabandi, "Antenna Miniaturization and Bandwidth Enhancement Using a Reactive Impedance Substrate", IEEE Transactions on Antennas and Propagation, Volume: 52, Issue: 9, pp. 2403-2414, Sept. 2004.

[32] S.D. Targonski ; R.B. Waterhouse ; D.M. Pozar. "Design of Wide-band Aperture-stacked Patch Microstrip Antennas", IEEE Transactions on Antennas and Propagation, Volume: 46, Issue: 9, pp. 1245-1251, Sep 1998.

[33] D.M. Pozar, B. Kaufman, "Increasing the bandwidth of a microstrip antenna by proximity coupling", Elect. Lett., vol. 23, no. 8, pp. 368-369, Apr 1987.

[34] W.S.T. Rowe, R.B. Waterhouse, "Investigation into the performance of proximity coupled stacked patches", IEEE Trans. Antennas Propag. vol. 54, no. 6, pp. 1693-1698, Jun 2006.

[35] B.W. Lim, E. Korolkiewicz , S. Scott, "Optimized design of corner microstrip fed nearly square patch antenna for circular polarization", Electronics Letters, Volume: 32, Issue: 7, pp. 600-602, Mar 1996.

[36] S.D.Targonski and D.M.Pozar, "Design of wideband circularly polarized aperture coupled microstrip antennas," IEEE Transactions on Antennas Propagation, vol. 41, pp. 214-220, Feb. 1993.

[37] N.C.Karmakar and M.E.Bialkowski, "Circularly Polarized Aperture-Coupled Circular Microstrip Patch Antennas for L-Band Applications," IEEE Transactions on Antennas Propagation, Vol. 47, No. 5, pp. 933-940, May 1999.

[38] LEE, C.S., and NALBANDIAN, V.: 'Circularly Polarized Microstrip Antenna with A Single Coaxial Feed', IEEE Trans. Antennas Propagat., 1996, AP-44, pp. 1426-1427

[39] Choon Sae Lee, V. Nalbandian, "Planar circularly polarized microstrip antenna with a single feed", IEEE Transactions on Antennas and Propagation, Volume: 47, Issue: 6, pp. 1005-1007, Jun 1999.

[40] COLLIN, R.E.: 'Field Theory of Guided Waves' (IEEE Press, 1991)

[41] P.S Hall and C.M. Hall, “Coplanar corporate feed effects in microstrip patch array design,” IEE Proceeding on Microwaves, Antennas and Propag., Vol. 135, no.3, pp. 180-186. June 1988

[42] E. Levine, G. Malamed, S. Shtrikman, and D. Treves, “A Study of microstrip array antennas with the feed network” IEEE Transactions on Antennas and Propagation. Vol. 37, no. 4, pp. 426-434, Apr 1989

[43] D. M. Pozar and D.H. Schaubert, “Comparison of three series fed microstrip array geometries”, IEEE Antenna and Propagation Symposium Digest, ann arbor, MI 1993, pp. 728-731

[44] S. Chakraborty and U. Mukherjee “Comparative study of microstrip patch line feed and coaxial feed antenna design using genetic algorithms” International Conference on Computer and Communication Technology (ICCCT). Pp 203-208, Sep. 2011

[45] P. Bhartia, V. S. Rao and R. S. Tomar, Millimeter-wave microstrip and printed circuit antennas, Boston, MA: Artech House, 1991.

[46] Anand Lakshmanan, Choon Sae Lee, “A standing-wave microstrip array antenna”, IEEE, Antennas and Propagation Society International Symposium (APSURSI), July 2010.

[47] Choon Sae Lee, Mohamed Ezzat, Seongheon Jeong, “Single-layer dual microstrip-array antenna”, IEEE, Antennas and Propagation Society International Symposium (APSURSI), July 2014.

[48] Choon Sae Lee, Mohamed Ezzat, “Large microstrip array antenna with hybrid feed network of standing and traveling waves”, IEEE, Antennas and Propagation & USNC/URSI National Radio Science Meeting, July 2015.

[49] J. Huang, "A technique for an array to generate circular polarization with linearly polarized elements," IEEE Trans. Antennas Propag., vol. 34, pp. 1113-1124, Sept. 1986.

[50] U. R. Kraft, "An experimental study on 2×2 sequential-rotation arrays with circularly polarized microstrip radiators," IEEE Trans. Antennas Propag., vol. 45, no. 10, pp. 1459-1466, Oct. 2007.

[51] S. L. S. Yang, R. Chair, A. A. Kishk, K. F. Lee, K. M. Luk, "Study on sequential feeding networks for subarrays of circularly polarized elliptical dielectric resonator antenna," IEEE Trans. Antennas Propag., vol. 55, no. 2, pp. 321-333, Feb. 2007.